

SAW Parameters Analysis and Equivalent Circuit of SAW Device

Trang Hoang

*Faculty of Electrical-Electronics Engineering, University of Technology, HoChiMinh City
VietNam*

1. Introduction

Surface Acoustic Wave (SAW) devices, using interdigital electrodes, play a key role in today's telecommunication systems and are widely used as electronic filters, resonators, delay lines, convolvers or wireless identification systems (ID tags).

During the last three decades, demands set by the expansion of the telecommunication industry and many applications in sensor have resulted in the introduction of a new generation of the SAW devices. Consequently, the design of high performance SAW devices requires precise and efficient models, simulation tools. Several methods have been proposed for modeling, analyzing SAW devices. These include the impulse model, the equivalent circuit models, the coupling-of-mode (COM) model, P-matrix model, angular spectrum of waves models [1] and the Scattering Matrix approach that was presented by Coldren and Rosenberg [2]. While the impulse model is only a first order model, the other models include second order effects, e.g. reflections, dispersion, and charge distribution effects. Purely numerical methods have also been and are being developed by many authors [3]-[35], [41].

In this chapter, the method for calculating the SAW parameters, including modeling and simulation, is given.

Section 2 gives the calculation of SAW properties and analyses of different SAW device structures.

Section 3 presents the equivalent circuit of SAW delay line based on Mason model.

The equivalent circuit of SAW delay line based on Couple-Of-Mode theory is presented in section 4.

Based on section 3 and 4, section 5 shows comparison between using the equivalent circuit of SAW delay line device based on Mason model and COM theory. This model is useful and fast model for designing the SAW device.

2. Calculation of SAW parameters

2.1 SAW parameters

The most important parameter for SAW device design is the center frequency, which is determined by the period of the IDT fingers and the acoustic velocity. The governing equation that determines the operation frequency is:

$$f_0 = v_{SAW} / \lambda \quad (1)$$

where

λ is the wavelength, determined by the periodicity of the IDT and v_{SAW} is the acoustic wave velocity. For the technology being used in this research:

$$\lambda = p = \text{finger width} \times 4 \quad (2)$$

with the finger width (as shown in Figure 1) is determined by the design rule of the technology which sets the minimum metal to metal distance.

v_{SAW} is surface acoustic wave velocity.

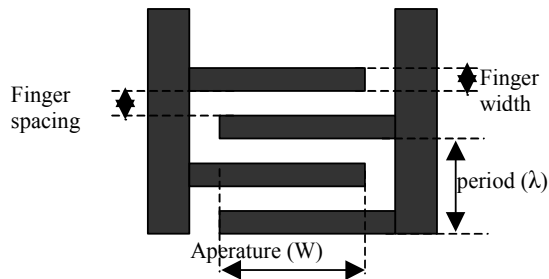


Fig. 1. IDT parameters

By using matrix method or Finite Element Method (FEM) in section 2.2, the velocity v of acoustic wave is derived in two cases:

- Wave velocity V_0 is velocity in case of free surface.
- Wave velocity V_s is velocity in case of short-circuit surface.

Therefore, the electromechanical coupling coefficient K is calculated approximately by Ingebrigtsen [54] as:

$$K^2 = 2 \frac{V_o - V_s}{V_o} \quad (3)$$

By using the matrix method or FEM and approximation of coupling factor as in (3), the SAW parameters in different structures AlN/Si, AlN/SiO₂/Si and AlN/Mo/Si are calculated and analysed in three next sections.

2.2 Matrix method and Finite Element Method (FEM). The choice between them

Matrix method

The SAW propagation properties on one layer or multilayer structure are obtained by using matrix approach, proposed by J.J.Campbell and W.R.Jones [50], K.A.Ingebrigtsen [54], and then developed by Fahmy and Adler [31], [32], [33] and other authors [51], [52], [53]. The numerical solution method is based on characterizing each layer by means of a transfer matrix relating the mechanical and electrical field variables at the boundary planes. The boundary conditions for multilayer are based on the mechanical and electrical field variables those quantities that must be continuous at material interfaces. This matrix method is used to calculate the wave velocity and therefore, the electromechanical coupling factor. A general view and detail of this approach are given as follows and also presented in [50]-[53].

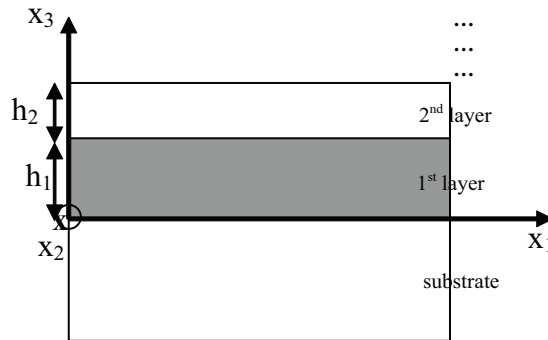


Fig. 2. Multilayer structure

Constitutive equations:

$$c_{ijkl} \frac{\partial^2 u_l}{\partial x_j \partial x_k} + e_{kij} \frac{\partial^2 \phi}{\partial x_j \partial x_k} = \rho \frac{\partial^2 u_i}{\partial t^2} \quad (4)$$

$$e_{jkl} \frac{\partial^2 u_l}{\partial x_j \partial x_k} - \varepsilon_{jk} \frac{\partial^2 \phi}{\partial x_j \partial x_k} = 0 \quad (5)$$

where

c_{ijkl} , e_{ijk} , ε_{jk} , ρ are elastic tensor, piezoelectric tensor, dielectric tensor and mass density, respectively, of the considered material.

U is the particle displacement.

ϕ is the scalar electric potential.

The boundary conditions are shown in Table 1

Position	Mechanical conditions	Electrical conditions
$x_3=0$	$U_i^S = U_i^{1st}$ $T_{3i}^S = T_{3i}^{1st}$	Boundary is open $\phi^S = \phi^{1st}$, $D^S = D^{1st}$ Boundary is short $\phi^S = \phi^{1st} = 0$
$x_3=h_1$	$U_i^{1st} = U_i^{2nd}$ $T_{3i}^{1st} = T_{3i}^{2nd}$	Boundary is open $\phi^{1st} = \phi^{2nd}$, $D^{1st} = D^{2nd}$ Boundary is short $\phi^{1st} = \phi^{2nd} = 0$
$x_3=h_1 + h_2$	$T_{3i}^{2nd} = 0$	Boundary is open $D^{2nd} = -\varepsilon.k.\phi^{2nd}$ Boundary is short $\phi^{2nd} = 0$

Table 1. Boundary conditions

where D: electronic displacement,

$$D_k = \frac{\partial \phi}{\partial x_k} \tag{6}$$

The general solution for U_l and ϕ (1) and (2) may be written as follows:

$$U_l = \sum_{m=1}^n C_m A_l^{(m)} \exp[ik(b^{(m)}x_3 + x_1 - vt)] \tag{7}$$

where $l = 1, 2, 3$

$$\phi = \sum_{m=1}^n C_m A_4^{(m)} \exp[ik(b^{(m)}x_3 + x_1 - vt)] \tag{8}$$

The coefficients C_m are determined from boundary conditions.

By substituting (7) and (8) in every layer into the boundary conditions, we have general form

$$[H] \begin{bmatrix} C_1^S \\ \dots \\ C_4^S \\ C_1^{1st} \\ \dots \\ C_8^{1st} \\ C_1^{2nd} \\ \dots \\ C_8^{2nd} \end{bmatrix} = 0 \tag{9}$$

Phase velocity is determined from the condition:

$$\text{Det}(H)=0 \tag{10}$$

(use approximation to solve (10))

Figure 3 shows the wave velocity of structure AlN/SiO₂(1.3μm)/Si(4μm).

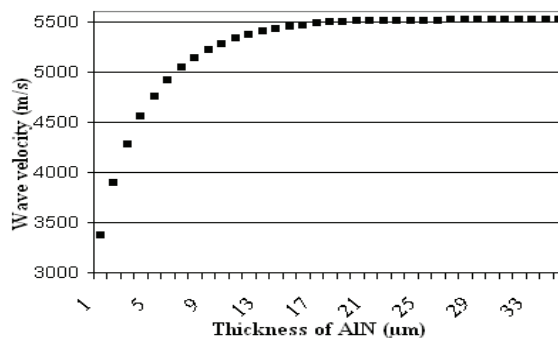


Fig. 3. Wave velocity in structure AlN/SiO₂(1.3μm)/Si(4μm) with different thicknesses of AlN

Finite Element Method (FEM)

In the design procedure of SAW devices, simple models like Equivalent Circuit Model coming from Smith Model and COM Model as presented above are used to achieve short calculation time and to get a general view of response of SAW devices. They are a good approach for designing SAW devices, for getting the frequency response, impedance parameters and transfer characteristics of SAW device. They could allow the designer to determine the major dimensions and parameters in number of fingers, finger width, and aperture. However, they are subjected to some simplifications and restrictions.

Field theory is the most appropriate theory for the design SAW devices as it involves the resolution of all the partial differential equations for a given excitation. The Finite Element Model (FEM) is the most appropriate numerical representation of field theory where the piezoelectric behaviour of the SAW devices can be discretized [45], [46]. Besides, nowadays, FEM tools also provide 3D view for SAW device, such as COMSOL® [47], Coventor® [48], ANSYS® [49].

The typical SAW devices can include a lot of electrodes (hundreds or even thousands of electrodes). In fact, we would like to include as many IDT finger pairs as possible in our FEM simulations. This would however significantly increase the scale of the device. Typically finite element models of SAW devices require a minimum of 20 mesh elements per wavelength to ensure proper convergence. A conventional two-port SAW devices consisting of interdigital transducers (IDT) may have – especially on substrate materials with low piezoelectric coupling constants - a length of thousands of wavelengths and an aperture of hundred wavelengths. Depending on the working frequency, the substrate which carries the electrode also has a depth of up to one hundred wavelengths. Taking into account that FEM requires a spatial discretization with at least twenty first order finite elements per wavelength and that an arbitrary piezoelectric material has at least four degrees of freedom, this leads to 8×10^8 unknowns in the three dimensional (3-D) case. Hence, the 3-D FEM representation of SAW device with hundreds of IDT fingers would require several million elements and nodes. The computational cost to simulate such a device is extremely high, or the amount of elements could not be handled by nowadays computer resources.

Fortunately, SAW devices consist of periodic section. M.Hofer et al proposed the Periodic Boundary Condition (PBC) in the FEM that allows the reduction of size of FE model tremendously [45], [46].

A good agreement between FEM and analytic method is obtained via the results in case of SAW with AlN thickness of $4\mu\text{m}$, wavelength of $8\mu\text{m}$ presented in Table 2.

	Matrix method	FEM	Difference between Matrix method and FEM (%)
f_0 (MHz)	771.13	775.48	0.56
f_s (MHz)	770.26	774.57	0.56
v_0 (m/s)	6169.02	6203.87	0.56
v_s (m/s)	6162.07	6196.54	0.56
K (%)	4.74	4.86	2.4

Table 2. Comparison between matrix method and FEM

From this table, matrix method and FEM give the same results. However, FEM would takes a long time and require a trial and error to find the results. Consequently, to reduce time, the matrix method proposed to be used to extract the parameters of SAW devices; FEM is

used to get a 3D view and explain some results that can not be explained by equivalent circuit. This point will be presented in next sections.

The three next sections present and analyse SAW parameters in different structures AlN/Si, AlN/SiO₂/Si and AlN/Mo/Si.

2.3 Wave velocity, coupling factor in AlN/Si structure

Figure 4 shows the dependence of Rayleigh wave velocity V_0 and V_s on the normalized thickness as respect to the wavelength, kh_{AlN} of AlN layer in SAW device AlN/Si substrate, where normalized thickness is defined by:

$$kh = \frac{2\pi h}{\lambda} \tag{11}$$

In this graph, when the normalized thickness of AlN, kh_{AlN} is larger than 3, the wave velocity reaches the velocity of the Rayleigh wave in AlN substrate $v_{(AlN \text{ substrate})}=6169$ (m/s). This could be explained that the wave travels principally in AlN layer when kh_{AlN} is larger than 3, because for low frequency the wave penetrates inside the other layer and this work is in the case where the wave are dispersive. It is better to be in the frequency range where the Rayleigh wave is obtained to have a constant velocity.

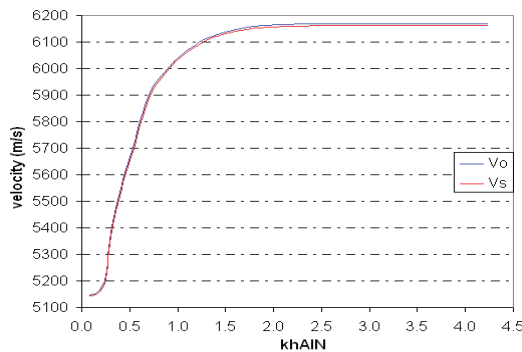


Fig. 4. Calculated values of wave velocity V_0 and V_s in SAW device AlN/Si substrate depend on the normalized thickness kh_{AlN} of AlN layer

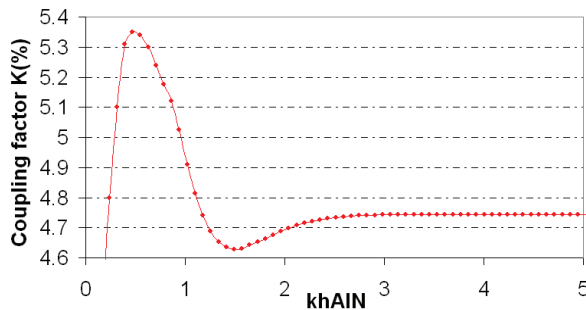


Fig. 5. Calculated values of coupling factor $K(\%)$ in SAW device AlN/Si substrate depends on the normalized thickness kh_{AlN} of AlN layer

The coupling factor K for this kind of device is shown in Figure 5. When normalized thickness of AlN layer is larger than 3, the coupling factor K still remain at 4.74% by that the wave travels principally in AlN layer.

In this configuration, K is at its maximum value of 5.34% when $kh_{AlN}=0.55$.

2.4 Wave velocity, coupling factor in AlN/SiO₂/Si structure

Wave velocity and coupling factor in structure AlN/SiO₂/Si are also presented in Figure 6 and Figure 7, respectively.

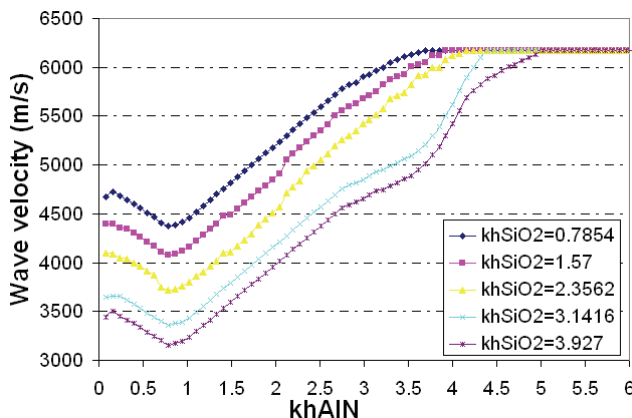


Fig. 6. Dependence of wave velocity in SAW device AlN/SiO₂/Si substrate on the normalized thickness kh_{AlN} of AlN layer and kh_{SiO_2}

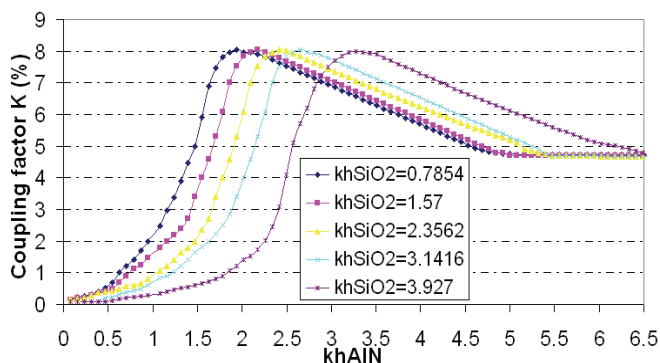


Fig. 7. Dependence of coupling factor $K(\%)$ in SAW device AlN/SiO₂/Si substrate on the normalized thickness kh_{AlN} of AlN layer and kh_{SiO_2}

In this configuration, as results in Figure 6, when $kh_{AlN} < 6$, with the same thickness of AlN layer, an increase in thickness of SiO₂ would decrease the wave velocity. When $kh_{AlN} > 6$, the wave velocity reaches the velocity of the Rayleigh wave in AlN substrate $v(AlN \text{ substrate})=6169$ (m/s). A same conclusion is formulated also for coupling factor for this kind of structure, AlN/SiO₂/Si, in Figure 7; when $kh_{AlN} > 6$, K remains at the value of 4.7%.

To understand the above behavior, we use FEM method to display displacement profile along the depth of multilayer AlN/SiO₂/Si. These results obtained from FEM method in case of $kh_{SiO_2}=0.7854$, $kh_{AlN}=5$ and $kh_{AlN}=0.2$ are compared as in Figure 8.

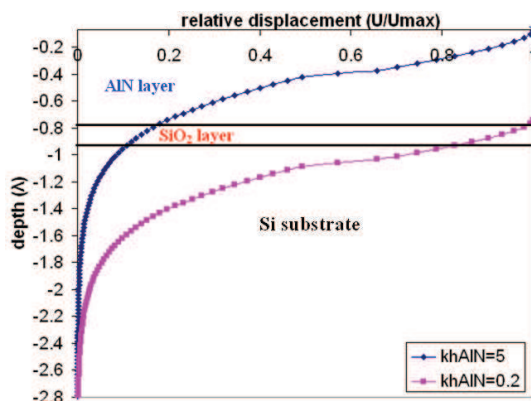


Fig. 8. Displacement profile along the depth of the multilayer AlN/SiO₂/Si, $kh_{SiO_2}=0.7854$

From Figure 8, we note that wave travels principally in AlN layer for a kh_{AlN} value of 5. By this reason, from a kh_{AlN} value of larger than 5, the coupling factor K remains at 4.7% and wave velocity remains at 6169m/s. For $kh_{AlN}=0.2$, wave travels principally in SiO₂ layer and Si substrate that are not piezoelectric layer. Consequently, the coupling factor K reaches the value of 0%.

In conclusion, the values of wave velocity and coupling factor depend on wave propagation medium, in which constant values of wave velocity and coupling factor indicate a large contribution of AlN layer, and coupling factor value of near 0% indicates a large contribution of SiO₂ layer and Si substrate.

2.5 Wave velocity, coupling factor in AlN/Mo/Si structure

For our devices, a thin Mo layer will be also deposited below the AlN layer to impose the crystal orientation of AlN. Besides this dependence, the Mo layer also has influences on

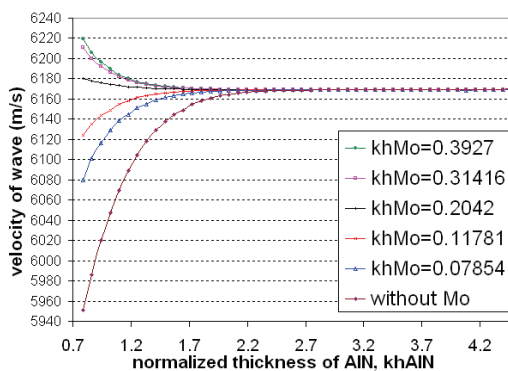


Fig. 9. Wave velocity AlN/Mo/Si substrate depends on the normalized thickness kh_{AlN} and kh_{Mo}

wave velocity and coupling factor K . These influences are shown in Figure 9 and Figure 10, respectively.

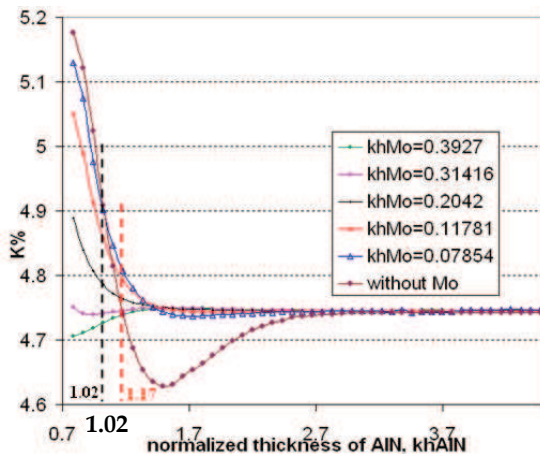


Fig. 10. Coupling factor K (%) in SAW device AlN/Mo/Si substrate depends on the normalized thickness kh_{AlN} and kh_{Mo}

From Figure 9, the use of Mo layer would increase the wave velocity with any thickness of AlN layer and Mo layer. In case of coupling factor K as in Figure 10, the Mo layer, however, could decrease K when the kh_{AlN} is less than 1.02. When the normalized thickness of AlN layer kh_{AlN} is in the range from 1.17 to 2.7, the Mo layer would increase the coupling factor K . And when the kh_{AlN} is larger than 2.7, the Mo has no influence on wave velocity and coupling factor. The reason of this effect could be explained by the displacement profile in AlN/Mo/Si structure, as shown in Figure 11 for thickness AlN value of $kh_{AlN}=2.7$. We could note that when $kh_{AlN} \geq 2.7$, the first interesting point is that the wave travels principally in AlN layer and Si substrate, the second one is that the relative displacement U/U_{max} in Mo layer will be smaller than 0.5. These points would explain the reason why when $kh_{AlN} \geq 2.7$ the use of Mo has no influence on wave velocity and coupling factor.

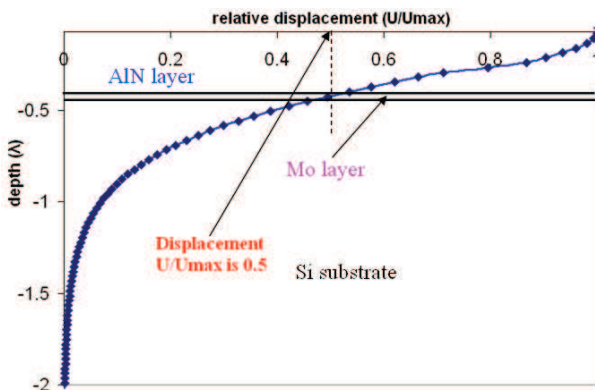


Fig. 11. Displacement profile along the depth of the multilayer AlN/Mo/Si, $kh_{AlN}=2.7$

3. Equivalent circuit for SAW delay line based on Mason model

3.1 Why Equivalent Circuit model is chosen?

Actual devices exist in a three-dimensional physical continuum. Their behaviour is governed by the laws of physics, chemistry, biology, and electronics. From a general point of view, the analysis of devices can be carried out by using some equations of laws of physics, chemistry ... For example; the analysis of piezoelectric resonators or transducers and their application to ultrasonic system can be solved by using the wave equation [36],[37]. But through analysis, equivalent electrical circuit representations of devices can be extracted. So, they can be readily expressible with Equivalent Electric Circuit. Below is the presentation of advantages and disadvantages of equivalent circuit.

Advantages:

- There are an immensely powerful set of intellectual tools to understand electric circuits.
- The equivalent circuit approach has distinct advantages over the direct physical, chemical equations approach (such as direct wave equations approach).
- Many theories, problems of electric circuits have already been solved such as microwave network theory, integrated circuit etc.
- Electric circuit approach is intrinsically correct from an energy point of view [56].
- A further advantage of electric circuit model is that it permits efficient modelling of the interaction between the electric and non-electric components of a microsystem. Both the electrical and mechanical portions of a system are represented by the same means. With software like Simulink, the block diagram is easily constructed, easily to build a more complex system but when we would like to connect a mechanical element to electrical circuits, Simulink can not do that. The analogies between electrical and mechanical elements are presented clearly by Warren P.Mason [57], [58].

Disadvantages:

- Care must be taken to make sure whether the boundary conditions are compatible with those used in the original derivation of the equivalent circuit [58].

In many systems, both commercial and industrial, pressure measurement plays a key role. Since pressure is a normal stress (force per unit area), pressure measurement can be done by using piezoelectric material which can convert stress into voltage. Equivalent circuits such as Mason's model [36] provide a powerful tool for the analysis and simulation of piezoelectric transducer elements. Most of the analogous circuits which have appeared in the literature implement transducers as the circuit elements. This model simulates both the coupling between the mechanical and electrical systems and the coupling between the mechanical and acoustical systems [39]. The mechanical, electrical and acoustic parts of piezoelectric transducer can be varied and analysed about behaviour by implementing equivalent circuits on computer tools such as Ansoft®, Spice, ADS, etc. For IDT composing of N periodic sections, Smith et al [41] developed the equivalent circuit model based on Berlincourt et al [40] work about equivalent circuit for Length Expander Bar with parallel electric field and with perpendicular electric field and based on the equivalent circuit for electromechanical transducer presented by Mason [36]. "Smith model" henceforth will be used to indicate this model. From this model, some models for SAW device in literature have been implemented. However, these models would include only IDTs [42], [43]. In SAW pressure sensor, one of sensitive parts is propagation path. It should be included in the model. The hybrid model based on Smith model for SAW pressure sensor which includes the IDTs and propagation path have been constructed.

Another equivalent model is based on the Coupling-Of-Modes (COM) theory. An excellent recent review of COM theory used in SAW devices was written by K.Hashimoto [10]. Based on the COM equations, as the force and voltage analogy can be used, the relationships between the terminal quantities at the one electrical port and two acoustic ports for an IDT have been done. K.Nakamura [44] introduced a simple equivalent circuit for IDT based on COM approach that is developed in section 4.

In conclusion, the equivalent-circuit model is chosen because it can allow fast design. This allows the designer to determine the major dimensions and parameters in number of fingers, fingers width, aperture, delay line distance, frequency response, impedance parameters and transfer characteristics of SAW device.

3.2 Equivalent circuit for IDT including N periodic sections

Based on Berlincourt et al [39] about equivalent circuit for Length Expander Bar with parallel electric field and with perpendicular electric field and based on the equivalent circuit for electromechanical transducer presented by Mason [36], Smith and al [41] have developed the equivalent circuit for IDT composed of N periodic sections of the form shown in Figure 12.

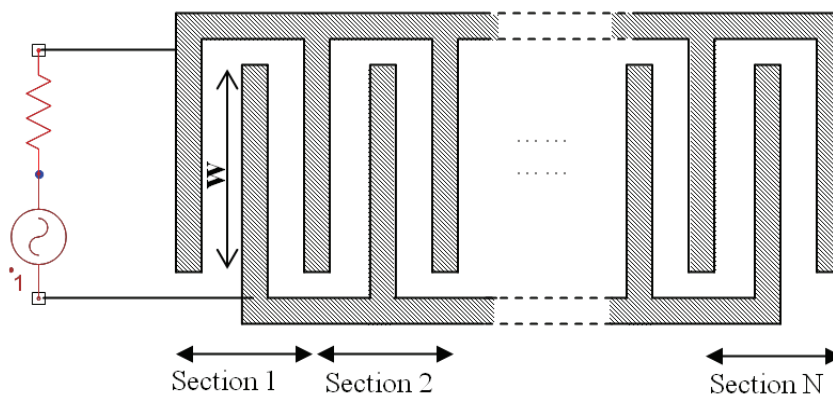


Fig. 12. Interdigital transducer diagram

One periodic section as shown in Figure 13 (a) can be presented by analogous one-dimensional configurations: “crossed-field” model as in Figure 13 (b), and “in-line” model as in Figure 13 (c). In “crossed-field” model, the applied electric field is normal to the acoustic propagation vector; while in “in-line field” model, the electric field is parallel to the propagation vector.

The important advantage of two one-dimensional models is that each periodic section can be represented by equivalent circuit of Mason, as shown in Figure 14 for “crossed-field” model and Figure 15 for “in-line field” model. The difference between these two equivalent circuits is that in “crossed-field” model, the negative capacitors are short-circuited.

Where:

$$\alpha = \frac{\theta}{4} = \frac{\pi \omega}{2 \omega_0} \quad (12)$$

With periodic section transit angle

$$\theta = 2\pi \frac{\omega}{\omega_0}$$

$$R_0 = \frac{2\pi}{\omega_0 C_s k^2} \tag{13}$$

R_0 is electrical equivalent of mechanical impedance Z_0 [59]

k : electromechanical coupling coefficient

$C_0=C_s/2$ with C_s : electrode capacitance per section

ω_0 is center angular frequency

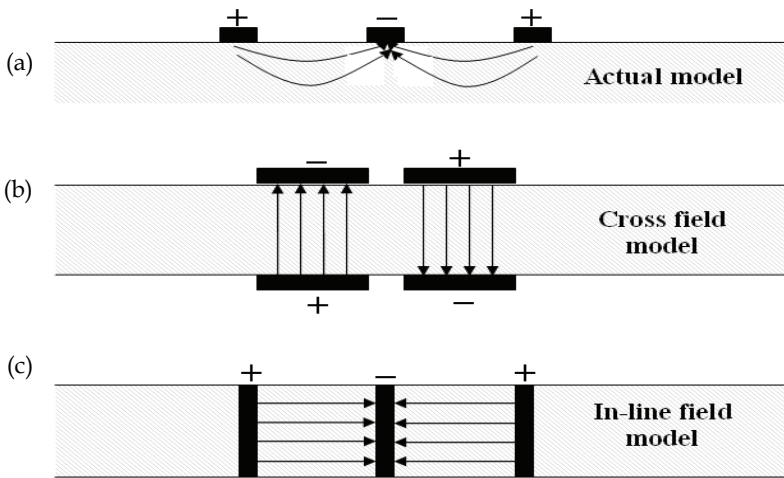


Fig. 13. Side view of the interdigital transducer and 2 analogous one-dimensional configurations (a) Actual model, (b) “crossed-field” model, (c) “in-line field” model

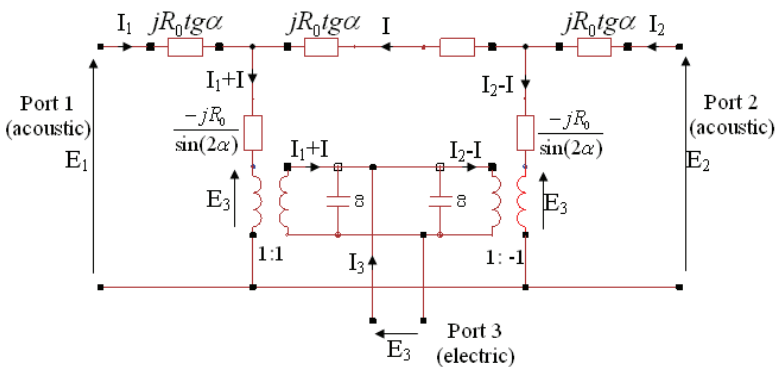


Fig. 14. Mason equivalent circuit for one periodic section in “crossed-field” model

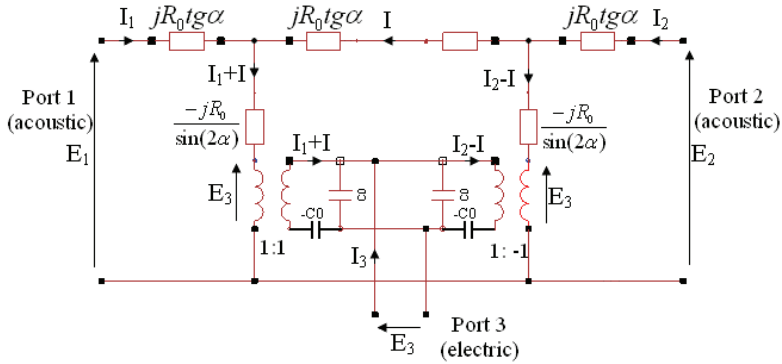


Fig. 15. Mason equivalent circuit for one periodic section in “in-line field” model

One periodic section can be represented by the 3-port network [y] matrix. The [y] matrix of one periodic section for 2 models as follows (see Appendix, section Appendix 1), with $G_0=R_0^{-1}$, R_0 is expressed by (13):

- for the “crossed-field” model:

$$\begin{aligned}
 y_{11} &= -jG_0 \cot g(4\alpha) \\
 y_{12} &= \frac{jG_0}{\sin(4\alpha)} \\
 y_{13} &= -jG_0 \operatorname{tg} \alpha \\
 y_{33} &= j(2\omega C_0 + 4G_0 \operatorname{tg} \alpha)
 \end{aligned}
 \tag{14}$$

- for the “in-line field” model:

$$\begin{aligned}
 y_{11} &= -jG_0 \cot g \alpha \left(\frac{G_0}{\omega C_0} - \cot g(2\alpha) \right) \left[2 - \frac{\left(\frac{G_0}{\omega C_0} - \frac{1}{\sin(2\alpha)} \right)^2}{\left(\frac{G_0}{\omega C_0} - \cot g(2\alpha) \right)^2} \right] \\
 y_{12} &= jG_0 \frac{\cot g \alpha \left(\frac{G_0}{\omega C_0} - \frac{1}{\sin(2\alpha)} \right)^2}{2 \left(\frac{2G_0}{\omega C_0} - \cot g \alpha \right) \left(\frac{G_0}{\omega C_0} - \cot g(2\alpha) \right)} \\
 y_{13} &= -jG_0 \frac{\operatorname{tg} \alpha}{1 - \frac{2G_0}{\omega C_0} \operatorname{tg} \alpha} \\
 y_{33} &= \frac{j2\omega C_0}{1 - \frac{2G_0}{\omega C_0} \operatorname{tg} \alpha}
 \end{aligned}
 \tag{15}$$

In IDT including N periodic sections, the N periodic sections are connected acoustically in cascade and electrically in parallel as represented in Figure 16.

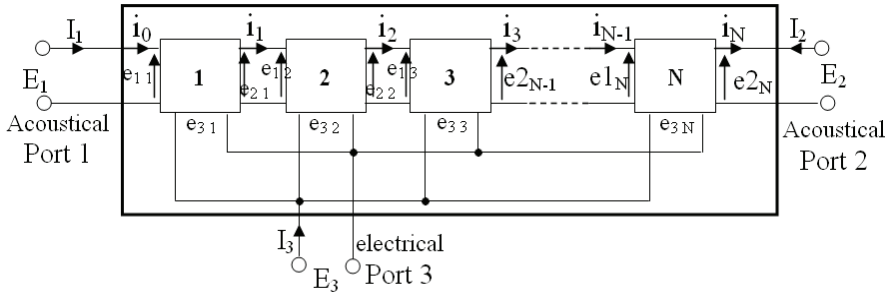


Fig. 16. IDT including the N periodic sections connected acoustically in cascade and electrically in parallel

Matrix [Y] representation of N-section IDT for two models, “crossed-field” model and “in-line” model are in (16) and (17), respectively (the calculation development is presented in Appendix, section Appendix 1):

- In "crossed-field" model:

$$\begin{aligned}
 Y_{11} &= -jG_0 \cot g(4N\alpha) \\
 Y_{12} &= \frac{jG_0}{\sin(4N\alpha)} \\
 Y_{13} &= -jG_0 \operatorname{tg}\alpha \\
 Y_{33} &= jN(2\omega C_0 + 4G_0 \operatorname{tg}\alpha)
 \end{aligned}
 \tag{16}$$

- In "in-line field" model:

$$\begin{aligned}
 Y_{11} &= -\frac{Q_{11}}{Q_{12}} \\
 Y_{12} &= \frac{1}{Q_{12}} \\
 Y_{13} &= -jG_0 \frac{\operatorname{tg}\alpha}{1 - \frac{2G_0}{\omega C_0} \operatorname{tg}\alpha} \\
 Y_{33} &= \frac{j2\omega N C_0}{1 - \frac{2G_0}{\omega C_0} \operatorname{tg}\alpha}
 \end{aligned}
 \tag{17}$$

It was shown in the literature that the crossed field model yielded better agreement than the experiment when compared to the in-line model when K is small. In section 2, K is always smaller than 7.2%. Besides, in section stated above, the “crossed-field” model is simpler than “in-line field” model in term of equations of all element of [Y] matrix. Consequently, the “crossed-field” model is selected henceforth for the calculating, modeling the devices.

3.3 Equivalent circuit for propagation path

The delay line SAW device could be used for pressure sensor application. The sensitive part of this kind of device will be the propagation path. To model the pressure sensor using

SAW, it is necessary to construct the model for propagation path. Based on the equivalent circuit for electromechanical transducer presented by Mason [36], equivalent circuit of propagation path is presented as in Figure 17.

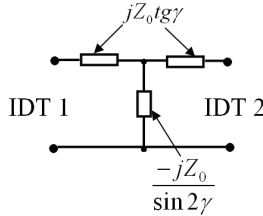


Fig. 17. Equivalent circuit of propagation path, based on Mason model

Where

$$\gamma = \frac{\omega l}{2v} \tag{18}$$

with v is SAW velocity, l is propagation length.

3.4 Equivalent circuit for SAW delay line

Due to the piezoelectric effect, an RF signal applied at input IDT stimulates a micro-acoustic wave propagating on its surface. These waves propagate in two directions, one to receiving IDT and another to the medium. The approximations as follows are assumed to construct the equivalent circuit for SAW delay line:

- Assume that the IDT radiates the wave into a medium of infinite extent. Experimentally, an infinite medium is approximated either by using absorber, such as wax, polyimide to provide acoustic termination, or by using a short RF pulse measurement. The condition of infinite medium means that no wave reflects back to input IDT. This is created for SAW device model by connecting the acoustic characteristic admittance Y_0 to one terminal of IDT.
- Assume that the wave propagating to receiving IDT has no attenuation during propagation way between two IDTs. So, the propagation path between two IDTs can be expressed as the no-loss transmission line.

Based on these two approximations, the $[Y]$ matrix representation of IDT in section 3.2, and propagation path representation in section 3.3, the SAW delay line can be expressed as equivalent circuit as in Figure 18.

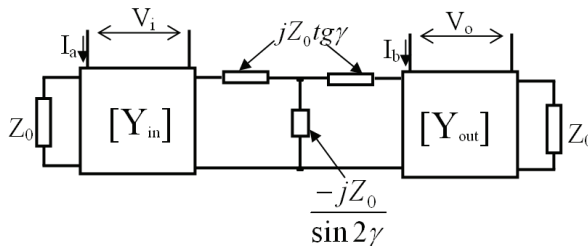


Fig. 18. Equivalent circuit of SAW delay line, based on Mason model

Section 3 gives the equivalent circuit of SAW delay line, including IDT input, IDT output and propagation path. All of calculation developments are presented in appendix, section 2. In this appendix, a new equivalent circuit of IDT including N periodic section plus one finger, which we call it “N+1/2”, also are developed and presented. Another representation of SAW delay line is [ABCD] matrix representation which also proposed in appendix, section Appendix 4. [ABCD] matrix representation has one interesting property that in cascaded network, the [ABCD] matrix of total network can be obtained easily by multiplying the matrices of elemental networks.

4. Equivalent circuit for IDT based on the Coupling-Of-Mode theory

The Coupling-Of-Modes formalism is a branch of the highly developed theory of wave propagation in periodic structure, which has an history of more than 100 years. This theory covers a variety of wave phenomena, including the diffraction of EM waves on periodic gratings, their propagation in periodic waveguides and antennas, optical and ultrasonic waves in multi-layered structures, quantum theory of electron states in metal, semiconductors, and dielectrics.... Theoretical aspects of the wave in periodic media and applications were reviewed by C.Elachi [4], in which it included theories of waves in unbounded and bounded periodic medium, boundary periodicity, source radiation in periodic media, transients in periodic structures, active and passive periodic structures, waves and particles in crystals. An excellent recent review of COM theory used in SAW devices was written by K.Hashimoto [10].

A simple equivalent circuit for IDT based on COM approach was proposed by K.Nakamura [29]. This model would be useful to analyze and design SAW devices. Based on the COM equations, the relationships between the terminal quantities at the one electrical port and two acoustic ports for an IDT have been done.

4.1 COM equation for particle velocities

Consider an IDT including N periodic sections with periodic length of L as shown in Figure 19.

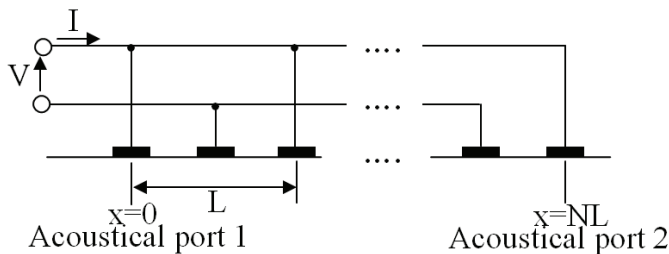


Fig. 19. IDT including N periodic sections

The particle velocities $v^+(x)$ and $v^-(x)$ of the wave propagating in the $+x$ and $-x$ directions in the periodic structure can be expressed as follows with the time dependence $\exp(j\omega t)$ term:

$$v^+(x) = A^+(x)e^{-jkx} \tag{19}$$

$$v^-(x) = A^-(x)e^{jkx} \tag{20}$$

Where k is the wave number

$$k = \omega / V_{SAW} \quad (21)$$

The amplitude $A^+(x)$ and $A^-(x)$ obey the following coupled-mode equations [60]:

$$\frac{dA^+(x)}{dx} = -jK_{11}A^+(x) - jK_{12}e^{j2\delta x}A^-(x) + j\zeta e^{j\delta x}V \quad (22)$$

$$\frac{dA^-(x)}{dx} = jK_{12}e^{-j2\delta x}A^+(x) + jK_{11}A^-(x) - j\zeta e^{-j\delta x}V \quad (23)$$

Where V is the voltage applied to the IDT,

ζ is the constant associated with the conversion from electrical to SAW quantities, K_{11} and K_{12} are coupling coefficients, sum of the coupling coefficient coming from the piezoelectric perturbation and that coming from the mechanical perturbation.

$$\delta = k - k_0, \text{ with } k_0 = \frac{2\pi}{L} \quad (24)$$

The solution to (22) and (23) can be expressed as

$$v^+(x) = (h_1 e^{-j\beta_1 x} + ph_2 e^{-j\beta_2 x} + q\zeta V) e^{-jk_0 x} \quad (25)$$

$$v^-(x) = (ph_1 e^{-j\beta_1 x} + h_2 e^{-j\beta_2 x} + q\zeta V) e^{jk_0 x} \quad (26)$$

Where the subscripts 1 and 2 indicate the elementary waves with wavenumbers $k_0 + \beta_1$ and $k_0 + \beta_2$ in the $+x$ direction, and the magnitudes h_1 and h_2 , respectively.

$$\beta_1, \beta_2 = \pm \sqrt{(\delta + K_{11})^2 - K_{12}^2} \quad (27)$$

$$p = \frac{\beta_1 - \delta - K_{11}}{K_{12}} \quad (28)$$

$$q = \frac{1}{\delta + K_{11} + K_{12}} \quad (29)$$

4.2 Equivalent circuit for IDT based on COM theory

From the equations (25) and (26), the particle velocities at the both ends of the IDT can be expressed as:

$$v^+(0) = h_1 + ph_2 + q\zeta V \quad (30)$$

$$v^-(0) = ph_1 + h_2 + q\zeta V \quad (31)$$

$$v^+(NL) = \pm (e^{-j\beta_1 NL} h_1 + e^{j\beta_1 NL} ph_2 + q\zeta V) \quad (32)$$

$$v^-(NL) = \pm(e^{-j\beta_1 NL} p h_1 + e^{j\beta_1 NL} h_2 + q\zeta V) \tag{33}$$

The upper and lower signs in (32) and (33) correspond to the cases $N=i$ and $N=i+0.5$, respectively, where i is an integer. Consequently, the total particle velocities at the two acoustical ports can be expressed as:

- Particle velocity at port 1 ($x=0$):

$$v_1 = v^+(0) + v^-(0) = (1+p)(h_1 + h_2) + 2q\zeta V \tag{34}$$

- Particle velocity at port 2 ($x=NL$):

$$v_2 = -[v^+(NL) + v^-(NL)] = \mp[(1+p)(e^{-j\beta_1 NL} h_1 + e^{j\beta_1 NL} h_2) + 2q\zeta V] \tag{35}$$

The two forces at two acoustic ports are considered to be proportional to the difference of v^+ and v^- . For the simplicity, these forces can be expressed as follows:

$$F_1 = v^+(0) - v^-(0) = (1-p)(h_1 - h_2) \tag{36}$$

$$F_2 = v^+(NL) - v^-(NL) = \pm[(1-p)(e^{-j\beta_1 NL} h_1 - e^{j\beta_1 NL} h_2)] \tag{37}$$

From these equations, h_1 and h_2 are the terms of F_1 and F_2 as follows:

$$h_1 = \frac{e^{j2\beta_1 NL}}{(1-p)(e^{j2\beta_1 NL} - 1)} F_1 \mp \frac{e^{j\beta_1 NL}}{(1-p)(e^{j2\beta_1 NL} - 1)} F_2 \tag{38}$$

$$h_2 = \frac{1}{(1-p)(e^{j2\beta_1 NL} - 1)} F_1 \mp \frac{e^{j\beta_1 NL}}{(1-p)(e^{j2\beta_1 NL} - 1)} F_2 \tag{39}$$

The current I at the electrical ports can be expressed as:

$$\begin{aligned} I &= \eta \int_0^{NL} [(1+p)(h_1 e^{-j\beta_1 x} + h_2 e^{-j\beta_2 x}) + 2q\zeta V] dx + j\omega N C_s V \\ &= j\eta \left\{ (1+p) \left[\frac{h_1}{\beta_1} (e^{-j\beta_1 NL} - 1) + \frac{h_2}{\beta_2} (e^{j\beta_1 NL} - 1) \right] \right\} + 2q\zeta \eta N L V + j\omega N C_s V \end{aligned} \tag{40}$$

where η is the constant associated with the convention from SAW to electrical quantities, therefore associated with the coupling factor K .

C_s is the capacitance for one electrode pair.

By substituting equations (38) and (39) in (34), (35) and (40), the following equations can be obtained:

$$I = (j\omega N C_s + 2q\zeta \eta N L) V + \frac{\eta(1+p)}{j\beta(1-p)} F_1 \mp \frac{\eta(1+p)}{j\beta(1-p)} F_2 \tag{41}$$

$$v_1 = 2q\zeta V + \frac{1+p}{1-p} \frac{1}{j \tan 2\theta} F_1 \mp \frac{1+p}{1-p} \frac{1}{j \sin 2\theta} F_2 \tag{42}$$

$$v_2 = \mp 2q\zeta V \mp \frac{1+p}{1-p} \frac{1}{j \sin 2\theta} F_1 + \frac{1+p}{1-p} \frac{1}{j \tan 2\theta} F_2 \quad (43)$$

Where

$$\theta = \beta NL / 2 \quad (44)$$

$$\beta \equiv \beta_1 = -\beta_2 \quad (45)$$

From these equations, the matrix as follows can be obtained:

$$\begin{bmatrix} I \\ v_1 \\ v_2 \end{bmatrix} = \begin{bmatrix} (j\omega NC_s + 2q\zeta\eta NL) & \frac{\eta(1+p)}{j\beta(1-p)} & \mp \frac{\eta(1+p)}{j\beta(1-p)} \\ 2q\zeta & \frac{1+p}{1-p} \frac{1}{j \tan 2\theta} & \mp \frac{1+p}{1-p} \frac{1}{j \sin 2\theta} \\ \mp 2q\zeta & \mp \frac{1+p}{1-p} \frac{1}{j \sin 2\theta} & \frac{1+p}{1-p} \frac{1}{j \tan 2\theta} \end{bmatrix} \begin{bmatrix} V \\ F_1 \\ F_2 \end{bmatrix} \quad (46)$$

In the acoustic wave transducer using piezoelectric effect, the force and voltage analogy can be used. Therefore, the COM-based circuit of IDT as matrix in (46) can be considered as the reciprocal circuit. The reciprocity theorem states that if a voltage source E acting in one branch of a network causes a current I to flow in another branch of the network, then the same voltage source E acting in the second branch would cause an identical current I to flow in the first branch. By using this theorem in this case, replacing V and F_1 together, the same value I requirement leads the following equations:

$$2q\zeta = \frac{\eta(1+p)}{j\beta(1-p)} \quad (47)$$

$$\eta = 2j\zeta \quad (48)$$

From (46), (47), and (48), the matrix as in (46) becomes:

$$\begin{bmatrix} I \\ v_1 \\ v_2 \end{bmatrix} = \begin{bmatrix} j\omega C_T + \frac{\phi^2}{j2\theta Z_0} & \frac{\phi}{j2\theta Z_0} & \mp \frac{\phi}{j2\theta Z_0} \\ \frac{\phi}{j2\theta Z_0} & \frac{1}{jZ_0 \tan 2\theta} & \mp \frac{1}{jZ_0 \sin 2\theta} \\ \mp \frac{\phi}{j2\theta Z_0} & \mp \frac{1}{jZ_0 \sin 2\theta} & \frac{1}{jZ_0 \tan 2\theta} \end{bmatrix} \begin{bmatrix} V \\ F_1 \\ F_2 \end{bmatrix} \quad (49)$$

Where

$$Z_0 = \frac{1-p}{1+p} = \frac{1}{q\beta} \quad (50)$$

$$\phi = \eta NL = 2j\zeta NL \quad (51)$$

$$C_T = NC_s \quad (52)$$

Consequently, the simple equivalent circuit obtained for IDT with N electrode pairs is shown in Figure 20:

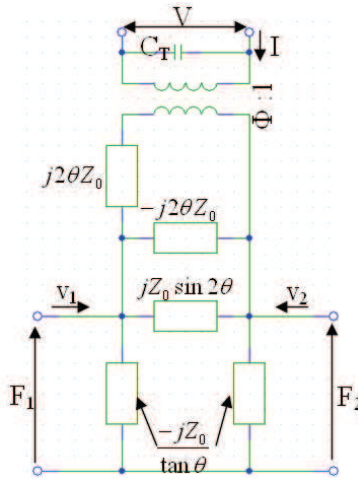


Fig. 20. Equivalent circuit IDT based on COM theory

4.3 Equivalent circuit for propagation path based on COM theory

In SAW devices, the propagation path should be taken into account. It is necessary to determine the equivalent circuit for a propagation path of distance l between 2 IDTs. This propagation path is a uniform section of length l , with a free surface or a uniformly metallized surface. In this case, $K_{11}=K_{12}=0$, and $\beta=\delta$.

Consequently, from equations (38) and (39), h_1 and h_2 can be expressed as:

$$h_1 = \frac{e^{j2\beta l}}{e^{j2\beta l} - 1} F_1 - \frac{e^{j\beta l}}{e^{j2\beta l} - 1} F_2 \tag{53}$$

$$h_2 = \frac{1}{e^{j2\beta l} - 1} F_1 - \frac{e^{j\beta l}}{e^{j2\beta l} - 1} F_2 \tag{54}$$

And, the particle velocities are expressed as:

$$v^+(x) = h_1 e^{-j(k_0 + \beta_1)x} = h_1 e^{-jkx} \tag{55}$$

$$v^-(x) = h_2 e^{j(k_0 + \beta_1)x} = h_2 e^{jkx} \tag{56}$$

If the v_1, v_2, F_1 , and F_2 are defined as:

$$v_1 = v^+(0) + v^-(0) \tag{57}$$

$$v_2 = -[v^+(NL) + v^-(NL)] \tag{58}$$

$$F_1 = v^+(0) - v^-(0) \tag{59}$$

$$F_2 = v^+(NL) - v^-(NL) \quad (60)$$

Then, by expressing h_1 and h_2 in terms of F_1 and F_2 based on equations (53) and (54), the v_1 and v_2 become as follows:

$$v_1 = h_1 + h_2 = \frac{e^{j2\beta l} + 1}{e^{j2\beta l} - 1} F_1 - \frac{2e^{j\beta l}}{e^{j2\beta l} - 1} F_2 \quad (61)$$

$$v_2 = h_1 e^{-jkl} + h_2 e^{jkl} = \frac{2e^{j\beta l}}{e^{j2\beta l} - 1} F_1 - \frac{e^{j2\beta l} + 1}{e^{j2\beta l} - 1} F_2 \quad (62)$$

Using the relation between complex number and trigonometry, the v_1 and v_2 can be expressed as follows:

$$v_1 = \frac{1}{jZ_0' \tan 2\theta} F_1 - \frac{1}{jZ_0' \sin 2\theta} F_2 \quad (63)$$

$$v_2 = -\frac{1}{jZ_0' \sin 2\theta} F_1 + \frac{1}{jZ_0' \tan 2\theta} F_2 \quad (64)$$

Consequently, the equivalent circuit for propagation path can be represented by the π -circuit of Figure 21:

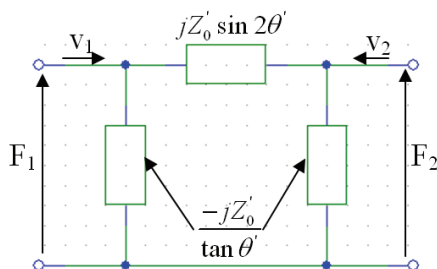


Fig. 21. Equivalent circuit of propagation path based on COM theory

Based on Mason model, the equivalent circuit of propagation path was presented in Figure 17, which has star form. In Figure 21, the circuit has triangle form. By using triangles and stars transformation theory published by A.E. Kennelly, equivalent circuit of propagation in these two figures is the same. Consequently, the approaches that are based on Mason model and COM theory can get the same equivalent circuit of propagation path.

4.4 Equivalent circuit for SAW delay line based on COM theory

Based on section 4.2 and 4.3, equivalent circuit of SAW delay line based on COM theory is presented in Figure 22.

In this model, some parameters must to be calculated or extracted. SAW velocity v , piezoelectric coupling factor K could be calculated from section 2. The periodic length L (or wavelength λ) is determined by design and fabrication.

The parameters K_{11} and K_{12} are coupling coefficients. They are sum of the coupling coefficient coming from the piezoelectric perturbation and that coming from the mechanical perturbation, and their equations for calculation are complicated [55]. Exact equations for

K_{11} and K_{12} were given by Y.Suzuki et al [55], but it seems so complex that their usefulnesses could be limited. However, from this work of Y.Suzuki et al [55], we propose the K_{11} and K_{12} could be expressed as follows:

$$K_{11} = O_{11}K^2k_0 \tag{65}$$

$$K_{12} = O_{12}K^2k_0 \tag{66}$$

Where k_0 is stated by (24) $k_0 = \frac{2\pi}{L}$ and K is piezoelectric coupling factor.

O_{11} is so-called self-coupling constant of finger, and O_{12} is so-called coupling constant between fingers. O_{12} could also presents the reflective wave between two fingers.

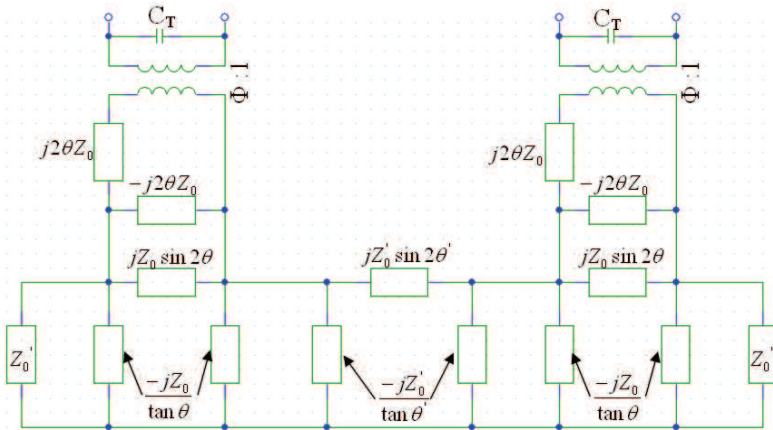


Fig. 22. Equivalent circuit of SAW delay line based on COM theory

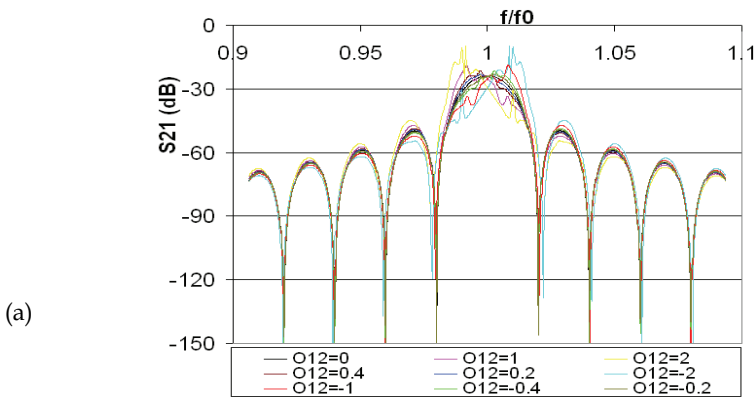


Fig. 23. Effect of O_{12} on S_{21} (dB), $N=50$, $v_{SAW}=5120\text{m/s}$, $\lambda=8\mu\text{m}$, $K=0.066453$, $O_{11}=0$

Figure 23 shows the effects of O_{12} on S_{21} (dB) of SAW device $N=50$, $v_{SAW}=5120\text{m/s}$, $\lambda=8\mu\text{m}$, $K=0.066453$ when $O_{11}=0$. S_{21} is the transmission coefficient in the scattering matrix representation [28].

Figure 24 shows the effects of O_{11} on S_{21} (dB) of SAW device $N=50$, $v_{SAW}=5120\text{m/s}$, $\lambda=8\mu\text{m}$, $K=0.066453$ when $O_{12}=0$. So, O_{11} coefficient shifts the center frequency of SAW device, the positive value of O_{11} reduces the center frequency f_0 of device, the negative on will increase the f_0 .

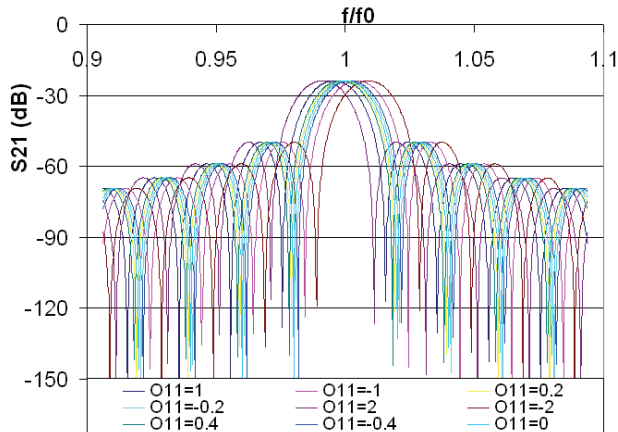


Fig. 24. Effect of O_{11} on S_{21} (dB), $N=50$, $v_{SAW}=5120\text{m/s}$, $\lambda=8\mu\text{m}$, $K=0.066453$, $O_{12}=0$

The effect of K_{11} and K_{12} could be explained by their measurement method [61]. K_{11} could be derived from the measurement of frequency response, therefore the usefulness of its calculation could be limited. Meanwhile, K_{12} can be extracted from FEM. It is shown in literature that K_{12} depends on the thickness of finger with respect to the wavelength. In our work, the ratio thickness/wavelength (its maximum value is $300\text{nm}/8\mu\text{m}$) is too small that its effect can be ignored. In conclusion, in our work, value of K_{11} and K_{12} are 0.

5. Comparison of equivalent circuit of SAW device based on Mason model and COM theory

Figure 25 presents the comparison between hybrid model and COM model in that $O_{11}=O_{12}=0$, distance between 2 IDTs is 50λ . These models could be the same, except that a

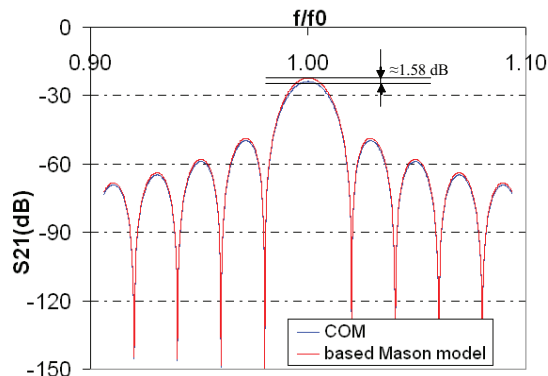


Fig. 25. Comparison between Hybrid model and COM model ($O_{11}=O_{12}=0$)

small difference in the peak value of S21 (dB) occurs. This difference could be explained by using “crossed-filed” model instead of actual model as in Figure 13.

6. Conclusion

The model used for SAW pressure sensor based on delay line are presented. For usefulness and reduction of time in design process, the equivalent circuit based on COM model, in which $K_{11}, K_{12}=0$ is proposed to be used.

Acoustic wave properties in different structures of AlN/SiO₂/Si, AlN/Si, and AlN/Mo/Si are analyzed. The wave velocity, coupling factor could depend on the wave propagation medium.

From analyses of these structures, the range in which there is a weak dependence of the wave velocity, coupling factor on the AlN layer thickness could be known. The SAW devices should be fabricated in this range to facilitate manufacturing.

For AlN/Si structure, this range is $kh_{AlN} \geq 3$.

For AlN/Mo/Si, if this kind of SAW device is fabricated in the range from $kh_{AlN} \geq 2.7$ to facilitate manufacturing, the use of Mo layer is useless. Consequently, to take full advantage of using Mo layer in term of wave velocity and coupling factor, it should be required to control the fabrication process carefully to obtain the required AlN thickness from $kh_{AlN}=1.02$ to $kh_{AlN}=2.7$.

For AlN/SiO₂/Si, this range is $kh_{AlN} \geq 5$ for $kh_{SiO_2}=0.7854$, for thicker SiO₂ layer, this range changes based on Figure 6 and Figure 7. Besides, using SiO₂ layer would reduce temperature dependence of frequency. To choose the thickness of SiO₂ layer, it would consider the effect of temperature dependence and analyses of wave velocity, coupling factor.

7. Appendix: Development of calculation for equivalent circuit of SAW device

7.1 Appendix 1. Equivalent circuit for normal IDT including N periodic sections

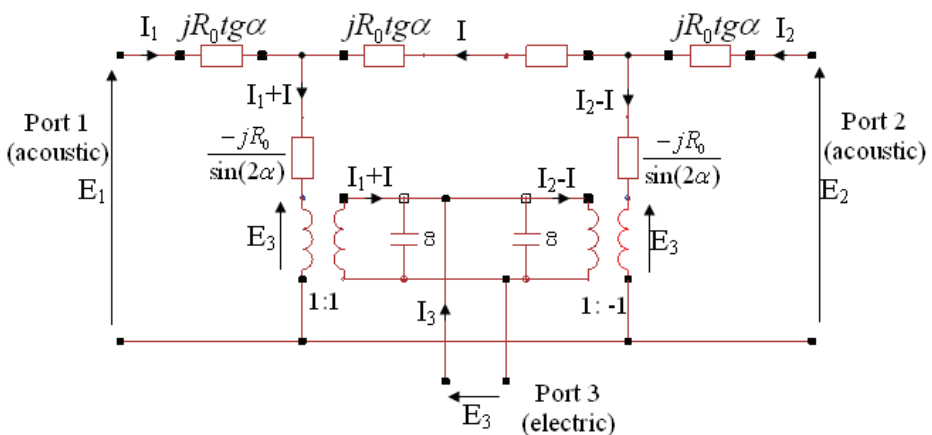


Fig. Appendix.1. Mason equivalent circuit for one periodic section in “crossed-field” model

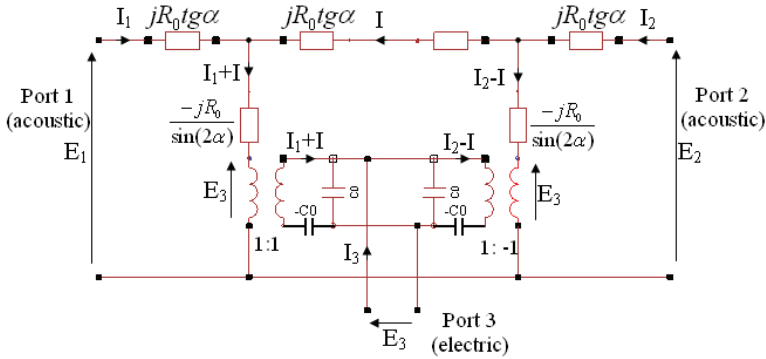


Fig. Appendix.2. Mason equivalent circuit for one periodic section in “in-line field” model
 One periodic section can be expressed by the 3-port network as follows:

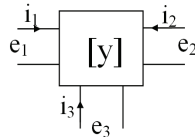


Fig. Appendix.3. One periodic section represented by 3-port network, admittance matrix [y]

$$\begin{bmatrix} i_1 \\ i_2 \\ i_3 \end{bmatrix} = \begin{bmatrix} y_{11} & y_{12} & y_{13} \\ y_{21} & y_{22} & y_{23} \\ y_{31} & y_{32} & y_{33} \end{bmatrix} \begin{bmatrix} e_1 \\ e_2 \\ e_3 \end{bmatrix} \tag{Appendix.1}$$

By the symmetrical properties of one periodic section (the voltage applied at port 3 will result in stress of the same value at port 1 and 2), the [y] matrix in (Appendix.1) becomes (Appendix.2) for Figure Appendix.4 and becomes (Appendix.3) for Figure Appendix.5.

$$\begin{bmatrix} i_1 \\ i_2 \\ i_3 \end{bmatrix} = \begin{bmatrix} y_{11} & y_{12} & y_{13} \\ y_{12} & y_{11} & -y_{13} \\ y_{13} & -y_{13} & y_{33} \end{bmatrix} \begin{bmatrix} e_1 \\ e_2 \\ e_3 \end{bmatrix} \tag{Appendix.2}$$

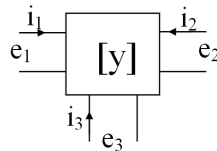


Fig. Appendix.4.
 3-port network representation of one periodic section, with the change of sign between Y_{13} and Y_{23} to ensure that acoustic power flows symmetrically away from transducer

$$\begin{bmatrix} i_1 \\ i_2 \\ i_3 \end{bmatrix} = \begin{bmatrix} y_{11} & y_{12} & y_{13} \\ -y_{12} & -y_{11} & y_{13} \\ y_{13} & -y_{13} & y_{33} \end{bmatrix} \begin{bmatrix} e_1 \\ e_2 \\ e_3 \end{bmatrix} \tag{Appendix.3}$$

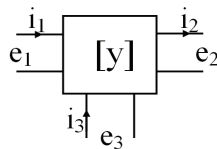


Fig. Appendix.5.
 3-port network representation of one periodic section, with the no change of sign between Y_{13} and Y_{23}

Applying circuit theory, definitions of [y] matrix elements are presented:

$$\begin{aligned} y_{11} &= \left. \frac{i_1}{e_1} \right|_{\substack{e_2=0 \\ e_3=0}} & ; & y_{12} &= \left. \frac{i_1}{e_2} \right|_{\substack{e_1=0 \\ e_3=0}} \\ y_{13} &= \left. \frac{i_1}{e_3} \right|_{\substack{e_1=0 \\ e_2=0}} & ; & y_{33} &= \left. \frac{i_3}{e_3} \right|_{\substack{e_1=0 \\ e_2=0}} \end{aligned} \quad (\text{Appendix.4})$$

And using trigonometric functions as follows:

$$\begin{aligned} \operatorname{tg} \alpha - \frac{2}{\sin(2\alpha)} &= -\cot g \alpha \\ \operatorname{tg} \alpha - \frac{1}{\sin(2\alpha)} &= \frac{1}{2}(\operatorname{tg} \alpha - \cot g \alpha) \\ \operatorname{tg} \alpha \frac{3 \cos(2\alpha) + 1 - \operatorname{tg} \alpha \sin(4\alpha) - \operatorname{tg} \alpha \sin(2\alpha)}{\operatorname{tg} \alpha \sin(4\alpha) + \operatorname{tg} \alpha \sin(2\alpha) - \cos(2\alpha)} &= -\operatorname{tg}(4\alpha) \end{aligned} \quad (\text{Appendix.5})$$

The [y] matrix can be obtained for 2 models as follows:

- for the “crossed-field” model:

$$\begin{aligned} y_{11} &= -jG_0 \cot g(4\alpha) \\ y_{12} &= \frac{jG_0}{\sin(4\alpha)} \\ y_{13} &= -jG_0 \operatorname{tg} \alpha \\ y_{33} &= j(2\omega C_0 + 4G_0 \operatorname{tg} \alpha) \end{aligned} \quad (\text{Appendix.6})$$

- for the “in-line field” model:

$$\begin{aligned} y_{11} &= -jG_0 \cot g \alpha \left(\frac{G_0}{\omega C_0} - \cot g(2\alpha) \right) \left[2 - \frac{\left(\frac{G_0}{\omega C_0} - \frac{1}{\sin(2\alpha)} \right)^2}{\left(\frac{G_0}{\omega C_0} - \cot g(2\alpha) \right)^2} \right] \\ y_{12} &= jG_0 \frac{\cot g \alpha \left(\frac{G_0}{\omega C_0} - \frac{1}{\sin(2\alpha)} \right)^2}{2 \left(\frac{2G_0}{\omega C_0} - \cot g \alpha \right) \left(\frac{G_0}{\omega C_0} - \cot g(2\alpha) \right)} \\ y_{13} &= -jG_0 \frac{\operatorname{tg} \alpha}{1 - \frac{2G_0}{\omega C_0} \operatorname{tg} \alpha} \\ y_{33} &= \frac{j2\omega C_0}{1 - \frac{2G_0}{\omega C_0} \operatorname{tg} \alpha} \end{aligned} \quad (\text{Appendix.7})$$

In IDT including N periodic sections, the N periodic sections are connected acoustically in cascade and electrically in parallel as Figure Appendix.6.

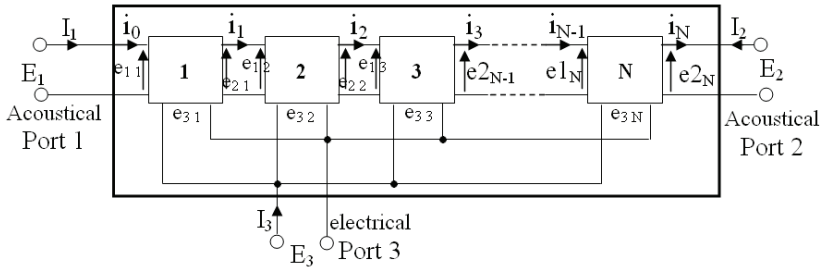


Fig. Appendix.6. IDT including the N periodic sections connected acoustically in cascade and electrically in parallel

Because the symmetric properties of the IDT including N section like these of one periodic section, and from (Appendix.2), (Appendix.3), Figure Appendix.4 and Figure Appendix.5, the [Y] matrices of N-section IDT are represented as follows:

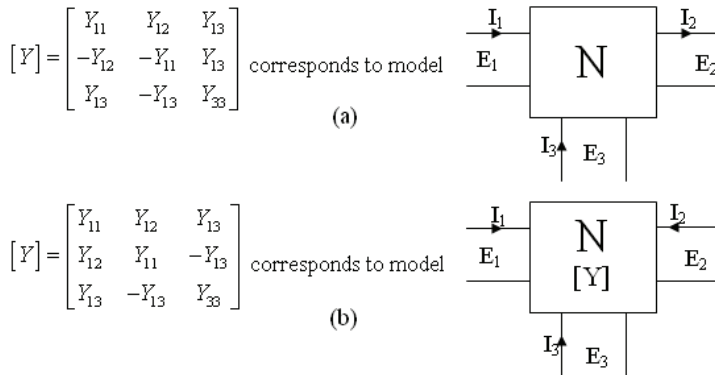


Fig. Appendix.7. The [Y] matrices and the model corresponditive models

Since the periodic sections are identical, the recursion relation as follows can be obtained:

$$e_{1m} = e_{2m-1} \tag{Appendix.8}$$

$$e_{3N} = e_{3N-1} = e_{3N-2} = \dots = e_{32} = e_{31} = E_3 \tag{Appendix.9}$$

$$i_{1m} = i_{2m-1} \tag{Appendix.10}$$

With m is integer number, $m=1,2, \dots, N-1, N$

The total transducer current is the sum of currents flowing into the N sections.

$$\begin{aligned}
 I_3 &= i_{31} + i_{32} + \dots + i_{3N-1} + i_{3N} \\
 &= (y_{13}e_{11} - y_{13}e_{21} + y_{33}e_{31}) + (y_{13}e_{12} - y_{13}e_{22} + y_{33}e_{32}) + \dots \\
 &\quad + (y_{13}e_{1N-1} - y_{13}e_{2N-1} + y_{33}e_{3N-1}) + (y_{13}e_{1N} - y_{13}e_{2N} + y_{33}e_{3N})
 \end{aligned}
 \tag{Appendix.11}$$

By applying (Appendix.8), (Appendix.9) and boundary conditions ($e_{11} = E_1$, $e_{2N}=E_2$), (Appendix.11) becomes:

$$I_3 = y_{13}e_{11} - y_{13}e_{2N} + N y_{33}E_3 = y_{13}E_1 - y_{13}E_2 + N y_{33}E_3 \quad (\text{Appendix.12})$$

From Figure Appendix.7, the Y_{13} and Y_{33} can be expressed as:

$$Y_{13} = y_{13} \quad (\text{Appendix.13})$$

$$Y_{33} = N y_{33} \quad (\text{Appendix.14})$$

Because the N periodic sections are connected acoustically in cascade and electrically in parallel, the model as in Figure Appendix.5 should be used to obtain the $[Y]$ matrix of N -section IDT.

From (Appendix.3) for one section, the i_1 and i_2 can be expressed

$$i_1 = y_{11}e_1 + y_{12}e_2 + y_{13}e_3, \quad i_2 = -y_{12}e_1 - y_{12}e_2 + y_{13}e_3 \quad (\text{Appendix.15})$$

Equations (Appendix.15) can be represented in matrix form like $[ABCD]$ form in electrical theory as follows:

$$\begin{bmatrix} e_2 \\ i_2 \end{bmatrix} = [K] \begin{bmatrix} e_1 \\ i_1 \end{bmatrix} + [L]e_3 \quad (\text{Appendix.16})$$

Where

$$[K] = \begin{bmatrix} -\frac{y_{11}}{y_{12}} & \frac{1}{y_{12}} \\ \frac{y_{11}^2 - y_{12}^2}{y_{12}} & -\frac{y_{11}}{y_{12}} \end{bmatrix} \quad (\text{Appendix.17})$$

$$[L] = \begin{bmatrix} -\frac{y_{13}}{y_{12}} \\ \frac{y_{11}y_{13} + y_{12}y_{13}}{y_{12}} \end{bmatrix} \quad (\text{Appendix.18})$$

By applying (Appendix.16) into N -section IDT as in Figure Appendix.6 and using (Appendix.9), the second recursion relation is obtained as follows:

$$\begin{bmatrix} e_m \\ i_m \end{bmatrix} = [K] \begin{bmatrix} e_{m-1} \\ i_{m-1} \end{bmatrix} + [L]E_3 \quad (\text{Appendix.19})$$

Where m is integer number, $m=1, 2, \dots, N-1, N$

Starting (Appendix.19)(Appendix.19) by using with $m=N$, and reducing m until $m=1$ gives the expression:

$$\begin{bmatrix} e_N \\ i_N \end{bmatrix} = [Q] \begin{bmatrix} e_0 \\ i_0 \end{bmatrix} + [X]E_3 \quad (\text{Appendix.20})$$

Where

$$[Q] = [K]^N \quad (\text{Appendix.21})$$

$$[X] = \begin{bmatrix} X_1 \\ X_2 \end{bmatrix} = \sum_{n=0}^{N-1} [K]^n [L] \quad (\text{Appendix.22})$$

Solving (Appendix.20) and using the boundary conditions ($e_0 = E_1, i_0 = I_1$) gives:

$$I_1 = -\frac{Q_{11}}{Q_{12}} E_1 + \frac{1}{Q_{12}} E_2 - \frac{X_1}{Q_{12}} E_3 \quad (\text{Appendix.23})$$

Consequently,

$$Y_{11} = -\frac{Q_{11}}{Q_{12}} \quad (\text{Appendix.24})$$

$$Y_{12} = \frac{1}{Q_{12}} \quad (\text{Appendix.25})$$

$$Y_{13} = -\frac{X_1}{Q_{12}} \quad (\text{Appendix.26})$$

The Y_{13} is known by (Appendix.13), so (Appendix.26) and matrix $[X]$ don't need to be solved.

To solve (Appendix.24) and (Appendix.25), matrix $[Q]$ should be solved.

In "crossed-field" model, matrix $[Q]$ can be represented in a simple form as follows:

$$[K] = \begin{bmatrix} \cos(4\alpha) & -jR_0 \sin(4\alpha) \\ -jG_0 \sin(4\alpha) & \cos(4\alpha) \end{bmatrix} \quad (\text{Appendix.27})$$

$$[K]^2 = \begin{bmatrix} \cos(8\alpha) & -jR_0 \sin(8\alpha) \\ -jG_0 \sin(8\alpha) & \cos(8\alpha) \end{bmatrix} \quad (\text{Appendix.28})$$

$$[K]^3 = \begin{bmatrix} \cos(12\alpha) & -jR_0 \sin(12\alpha) \\ -jG_0 \sin(12\alpha) & \cos(12\alpha) \end{bmatrix} \quad (\text{Appendix.29})$$

..... etc. Consequently, matrix $[Q]$ will be given:

$$[Q] = [K]^N = \begin{bmatrix} \cos(N4\alpha) & -jR_0 \sin(N4\alpha) \\ -jG_0 \sin(N4\alpha) & \cos(N4\alpha) \end{bmatrix} \quad (\text{Appendix.30})$$

From (Appendix.24) and (Appendix.35), Y_{11} and Y_{12} in "cross-field" model can be expressed:

$$Y_{11} = -jG_0 \cot g(N4\alpha) \quad (\text{Appendix.31})$$

$$Y_{12} = \frac{jG_0}{\sin(N4\alpha)} \quad (\text{Appendix.32})$$

In conclusion, matrix [Y] representation of N-section IDT is:

- In "crossed-field" model, from (Appendix.6), (Appendix.13), (Appendix.14), (Appendix.31) and (Appendix.32):

$$\begin{aligned}
 Y_{11} &= -jG_0 \cot g(4N\alpha) \\
 Y_{12} &= \frac{jG_0}{\sin(4N\alpha)} \\
 Y_{13} &= -jG_0 \operatorname{tg}\alpha \\
 Y_{33} &= jN(2\omega C_0 + 4G_0 \operatorname{tg}\alpha)
 \end{aligned}
 \tag{Appendix.33}$$

- In "in-line field" model, from (Appendix.7), (Appendix.13), (Appendix.14), (Appendix.24) and (Appendix.25):

$$\begin{aligned}
 Y_{11} &= -\frac{Q_{11}}{Q_{12}} \\
 Y_{12} &= \frac{1}{Q_{12}} \\
 Y_{13} &= -jG_0 \frac{\operatorname{tg}\alpha}{1 - \frac{2G_0}{\omega C_0} \operatorname{tg}\alpha} \\
 Y_{33} &= \frac{j2\omega NC_0}{1 - \frac{2G_0}{\omega C_0} \operatorname{tg}\alpha}
 \end{aligned}
 \tag{Appendix.34}$$

Where [Q] can be calculated from (Appendix.17) and (Appendix.21).

7.2 Appendix 2: Equivlent circuit for “N+1/2” model IDT

In case IDT includes N periodic sections (like in section 3.2 plus one finger (in color red) as shown in Figure Appendix.8 that we call “N+1/2” model IDT.

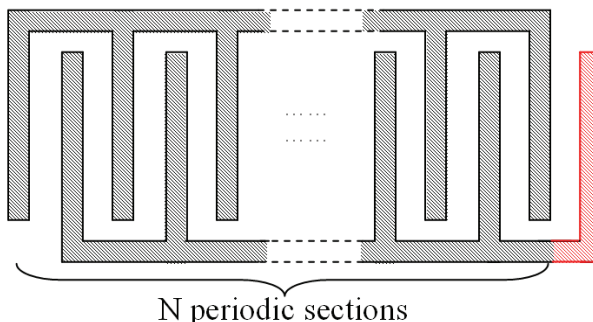


Fig. Appendix.8. “N+1/2” model IDT

The equivalent circuit for this model is shown in Figure Appendix.9 and the matrix [Yd] representation is shown as in Figure Appendix.10 (letter “d” stands for different from model [Y] in section 3.2.

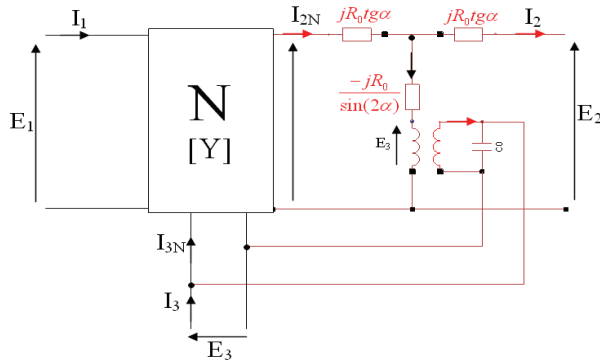


Fig. Appendix.9. Equivalent circuit of “N+1/2” model IDT

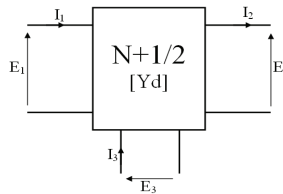


Fig. Appendix.10. [Yd] matrix representation of “N+1/2” model IDT

The form of matrix [Yd] is:

$$[Yd] = \begin{bmatrix} Yd_{11} & Yd_{12} & Yd_{13} \\ Yd_{21} & Yd_{22} & Yd_{23} \\ Yd_{31} & Yd_{32} & Yd_{33} \end{bmatrix} \tag{Appendix.35}$$

The elements of [Yd] matrix for “crossed-field” model are given as follows:

$$Yd_{11} = jG_0 \left\{ \frac{1}{\sin^2(4N\alpha)(\cot g(2\alpha) + \cot g(4N\alpha))} - \cot g(4N\alpha) \right\} \tag{Appendix.36}$$

$$Yd_{12} = \frac{jG_0}{\sin(4N\alpha)} \left\{ \cos(2\alpha) - \frac{\sin(2\alpha)[\cot g(4N\alpha)\cos(2\alpha) - \sin(2\alpha)]}{\cos(2\alpha) + \cot g(4N\alpha)\sin(2\alpha)} \right\} \tag{Appendix.37}$$

$$Yd_{13} = jG_0 \left\{ \frac{(-tg\alpha + 2\cot g(4N\alpha)\sin^2\alpha + \sin(2\alpha))\sin(2\alpha)}{\sin(4N\alpha)(\cos(2\alpha) + \cot g(4N\alpha)\sin(2\alpha))} + \frac{2\sin^2\alpha}{\sin(4N\alpha)} - tg\alpha \right\} \tag{Appendix.38}$$

$$Yd_{21} = -jG_0 \frac{1}{\sin(4N\alpha)(\cos(2\alpha) + \cot g(4N\alpha)\sin(2\alpha))} \tag{Appendix.39}$$

$$Yd_{22} = jG_0 \frac{\cot g(4N\alpha)\cos(2\alpha) - \sin(2\alpha)}{\cos(2\alpha) + \cot g(4N\alpha)\sin(2\alpha)} \tag{Appendix.40}$$

$$Yd_{23} = jG_0 \frac{-tg\alpha + 2 \cot g(4N\alpha) \sin^2(2\alpha) + \sin(2\alpha)}{\cos(2\alpha) + \cot g(4N\alpha) \sin(2\alpha)} \quad (\text{Appendix.41})$$

$$Yd_{31} = -jG_0 tg\alpha \quad (\text{Appendix.42})$$

$$Yd_{32} = -jG_0 \sin(2\alpha) \quad (\text{Appendix.43})$$

$$Yd_{33} = j\omega C_0(2N - 1) + jG_0 \{ \sin(2\alpha) + (4N + 1)tg\alpha \} \quad (\text{Appendix.44})$$

7.3 Appendix 3: Scattering matrix [S] for IDT

The scattering matrix [S] of a three-port network characterized by its admittance matrix [Y] is given by [3]:

$$S = \Pi_3 - 2Y(\Pi_3 + Y)^{-1} \quad (\text{Appendix.45})$$

Where Π_3 is the 3x3 identity matrix.

After expanding this equation, the scattering matrix elements for a general three-port network are given by the following expressions:

$$S_{11} = \frac{1}{M} \{ (1 + Y_{33})(1 - Y_{11} + Y_{22} - Y_{11}Y_{22} + Y_{12}Y_{21}) + Y_{13}[Y_{31}(1 + Y_{22}) - Y_{21}Y_{32}] + Y_{23}[Y_{32}(Y_{11} - 1) - Y_{12}Y_{31}] \} \quad (\text{Appendix.46})$$

$$S_{12} = -\frac{2}{M} [Y_{12}(1 + Y_{33}) - Y_{13}Y_{32}] \quad (\text{Appendix.47})$$

$$S_{13} = -\frac{2}{M} [Y_{13}(1 + Y_{22}) - Y_{12}Y_{23}] \quad (\text{Appendix.48})$$

$$S_{21} = -\frac{2}{M} [Y_{21}(1 + Y_{33}) - Y_{23}Y_{31}] \quad (\text{Appendix.49})$$

$$S_{22} = \frac{1}{M} \{ (1 + Y_{33})(1 + Y_{11} - Y_{22} - Y_{11}Y_{22} + Y_{12}Y_{21}) + Y_{13}[Y_{31}(Y_{22} - 1) - Y_{21}Y_{32}] + Y_{23}[Y_{32}(Y_{11} + 1) - Y_{12}Y_{31}] \} \quad (\text{Appendix.50})$$

$$S_{23} = -\frac{2}{M} [Y_{23}(1 + Y_{11}) - Y_{13}Y_{21}] \quad (\text{Appendix.51})$$

$$S_{31} = -\frac{2}{M} [Y_{31}(1 + Y_{22}) - Y_{21}Y_{32}] \quad (\text{Appendix.52})$$

$$S_{32} = -\frac{2}{M} [Y_{32}(1 + Y_{11}) - Y_{12}Y_{31}] \quad (\text{Appendix.53})$$

$$S_{33} = \frac{1}{M} \{ (1 - Y_{33})(1 + Y_{11} + Y_{22} + Y_{11}Y_{22} - Y_{12}Y_{21}) + Y_{13}[Y_{31}(Y_{22} + 1) - Y_{21}Y_{32}] + Y_{23}[Y_{32}(Y_{11} + 1) - Y_{12}Y_{31}] \} \quad (\text{Appendix.54})$$

where

$$M = \det(\Pi_3 + Y) \\ = (1 + Y_{33})[(1 + Y_{11})(1 + Y_{22}) - Y_{12}Y_{21}] - Y_{23}[Y_{32}(1 + Y_{11}) - Y_{12}Y_{31}] - \\ - Y_{13}[Y_{31}(1 - Y_{22}) - Y_{21}Y_{32}] \quad (\text{Appendix.55})$$

For model IDT including N identical sections, these equations can be further simplified. In case of Figure Appendix.7 (b):

$$\begin{aligned} Y_{11} &= Y_{22} \\ Y_{21} &= Y_{12} \\ Y_{31} &= Y_{13} \\ Y_{23} &= Y_{32} = -Y_{13} \end{aligned} \quad (\text{Appendix.56})$$

Therefore, S_{ij} 's take the following form

$$S_{11} = S_{22} = \frac{1}{M} \{ (1 + Y_{33})(1 - Y_{11}^2 + Y_{12}^2) + 2Y_{13}^2(Y_{11} + Y_{12}) \} \quad (\text{Appendix.57})$$

$$S_{12} = S_{21} = -\frac{2}{M} [Y_{12}(1 + Y_{33}) + Y_{13}^2] \quad (\text{Appendix.58})$$

$$S_{13} = S_{31} = -\frac{2}{M} Y_{13}(1 + Y_{11} + Y_{12}) \quad (\text{Appendix.59})$$

$$S_{23} = S_{32} = -S_{13} \quad (\text{Appendix.60})$$

$$S_{33} = \frac{1}{M} \{ (1 - Y_{33})[(1 + Y_{11})^2 - Y_{12}^2] + 2Y_{13}^2(1 + Y_{11} + Y_{12}) \} \quad (\text{Appendix.61})$$

Where

$$M = (1 + Y_{33})[(1 + Y_{11})^2 - Y_{12}^2] - 2Y_{13}^2(1 + Y_{12}) \quad (\text{Appendix.62})$$

7.4 Appendix 4: Equivalent circuit for SAW device base on Mason model, [ABCD]

Matrix representation

7.4.1 Appendix 4.1: [ABCD] Matrix representation of IDT

In SAW device, each input and output IDTs have one terminal connected to admittance G_0 . Therefore, one IDT can be represented as two-port network. [ABCD] matrix (as in Figure Appendix.11) is used to represent each IDT, because [ABCD] matrix representation has one interesting property that in cascaded network, the [ABCD] matrix of total network can be obtained easily by multiplying the matrices of elemental networks.

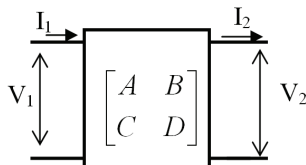


Fig. Appendix.11. [ABCD] representation of two-port network for one IDT

To find the [ABCD] matrix for one IDT in SAW device, the condition that no reflected wave at one terminal of IDT, and the current-voltage relations by [Y] matrix in section are used as follows:

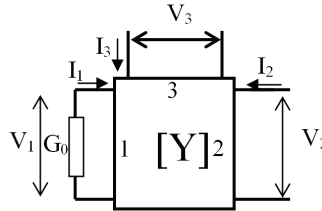


Fig. Appendix.12. Two-port network for one IDT

$$\begin{bmatrix} I_1 \\ I_2 \\ I_3 \end{bmatrix} = \begin{bmatrix} Y_{11} & Y_{12} & Y_{13} \\ Y_{12} & Y_{11} & -Y_{13} \\ Y_{13} & -Y_{13} & Y_{33} \end{bmatrix} \begin{bmatrix} V_1 \\ V_2 \\ V_3 \end{bmatrix} \tag{Appendix.63}$$

And $I_1 = -G_0 V_1$ (Appendix.64)

From these current-voltage relations, the V_3 and I_3 are given:

$$V_3 = \frac{Y_{11}^2 - Y_{12}^2 + Y_{11}G_0}{Y_{12}Y_{13} + Y_{11}Y_{13} + Y_{13}G_0} V_2 - \frac{G_0 + Y_{11}}{Y_{12}Y_{13} + Y_{11}Y_{13} + Y_{13}G_0} I_2 \tag{Appendix.65}$$

$$I_3 = \frac{-(Y_{13}Y_{12} + Y_{13}Y_{11} + Y_{13}G_0)^2 + (Y_{11}Y_{33} - Y_{13}^2 + Y_{33}G_0)(Y_{11}^2 - Y_{12}^2 + Y_{11}G_0)}{(G_0 + Y_{11})(Y_{12}Y_{13} + Y_{11}Y_{13} + Y_{13}G_0)} V_2 - \frac{Y_{11}Y_{33} - Y_{13}^2 + Y_{33}G_0}{Y_{12}Y_{13} + Y_{11}Y_{13} + Y_{13}G_0} I_2 \tag{Appendix.66}$$

From (Appendix.65) and (Appendix.66), equivalence between port 3 in Figure Appendix.12 equals to port 1 in Figure Appendix.11, and consideration of direction of current I_2 in Figure Appendix.11 and Figure Appendix.12, [ABCD] matrix representation for two-port network of IDT in obtained:

$$A = \frac{Y_{11}^2 - Y_{12}^2 + Y_{11}G_0}{Y_{12}Y_{13} + Y_{11}Y_{13} + Y_{13}G_0} \tag{Appendix.67}$$

$$B = \frac{G_0 + Y_{11}}{Y_{12}Y_{13} + Y_{11}Y_{13} + Y_{13}G_0} \tag{Appendix.68}$$

$$C = \frac{-(Y_{13}Y_{12} + Y_{13}Y_{11} + Y_{13}G_0)^2 + (Y_{11}Y_{33} - Y_{13}^2 + Y_{33}G_0)(Y_{11}^2 - Y_{12}^2 + Y_{11}G_0)}{(G_0 + Y_{11})(Y_{12}Y_{13} + Y_{11}Y_{13} + Y_{13}G_0)} \tag{Appendix.69}$$

$$D = \frac{Y_{11}Y_{33} - Y_{13}^2 + Y_{33}G_0}{Y_{12}Y_{13} + Y_{11}Y_{13} + Y_{13}G_0} \tag{Appendix.70}$$

In case of “crossed-field” model, the [ABCD] can be further simplified:

$$A = \frac{\sin(4N\alpha) - j \cos(4N\alpha)}{tg\alpha [1 - \cos(4N\alpha) - j \sin(4N\alpha)]} \quad (\text{Appendix.71})$$

$$B = \frac{A}{G_0} \quad (\text{Appendix.72})$$

$$D = \frac{\sin(4N\alpha)}{1 - \cos(4N\alpha) - j \sin(4N\alpha)} [N(2\alpha C_0 Z_0 \cot \alpha + 4)(\cot(4N\alpha) + j) + tg\alpha] \quad (\text{Appendix.73})$$

$$C = -\frac{1}{B} + G_0 D \quad (\text{Appendix.74})$$

One interesting property of [ABCD] of "crossed-field" mode is:

$$AD - BC = 1 \quad (\text{Appendix.75})$$

This means [ABCD] matrix is reciprocal.

In SAW device, the output IDT is inverse of input IDT. By the reciprocal property of [ABCD], the [ABCD] matrix of output IDT can be easily obtained:

$$A_{\text{output}} = D_{\text{input}} \quad (\text{Appendix.76})$$

$$B_{\text{output}} = B_{\text{input}} \quad (\text{Appendix.77})$$

$$C_{\text{output}} = C_{\text{input}} \quad (\text{Appendix.78})$$

$$D_{\text{output}} = A_{\text{input}} \quad (\text{Appendix.79})$$

in which N is replaced by M (number of periodic sections in output IDT)

Consequently, the [ABCD] matrix of output IDT is:

$$A_{\text{out}} = \frac{\sin(4M\alpha)}{1 - \cos(4M\alpha) - j \sin(4M\alpha)} [M(2\alpha C_0 Z_0 \cot \alpha + 4)(\cot(4M\alpha) + j) + tg\alpha] \quad (\text{Appendix.80})$$

$$B_{\text{out}} = \frac{1}{G_0} \frac{\sin(4M\alpha) - j \cos(4M\alpha)}{tg\alpha [1 - \cos(4M\alpha) - j \sin(4M\alpha)]} \quad (\text{Appendix.81})$$

$$D_{\text{out}} = \frac{\sin(4M\alpha) - j \cos(4M\alpha)}{tg\alpha [1 - \cos(4M\alpha) - j \sin(4M\alpha)]} \quad (\text{Appendix.82})$$

$$C_{\text{out}} = -\frac{1}{B_{\text{out}}} + G_0 A_{\text{out}} \quad (\text{Appendix.83})$$

At the center frequency f_0 , the [ABCD] matrix becomes infinite since $\alpha = 0.5\pi(f/f_0) = 0.5\pi$. However, [ABCD] elements may be calculated by expanding for frequency very near frequency f_0 .

By setting:

$$\alpha = \frac{\pi}{2} \frac{f - f_0}{f_0} + \frac{\pi}{2} = \frac{x}{2N} + \frac{\pi}{2} \quad (\text{Appendix.84})$$

Where
$$x = N\pi \frac{f - f_0}{f_0} \tag{Appendix.85}$$

By using the limit of some functions as follows:

$$\lim_{x \rightarrow 0} [\sin(4N\alpha)] = \lim_{x \rightarrow 0} [\sin(2x)] \approx 2x \tag{Appendix.86}$$

$$\lim_{x \rightarrow 0} [\cos(4N\alpha)] = \lim_{x \rightarrow 0} [\cos(2x)] \approx 1 \tag{Appendix.87}$$

$$\lim_{x \rightarrow 0} [tg\alpha] = \lim_{x \rightarrow 0} [-\cot(\frac{x}{2N})] \approx -\frac{2N}{x} \tag{Appendix.88}$$

The [ABCD] matrix of input IDT is obtained:

$$A \approx \frac{2x - j}{j4N} \tag{Appendix.89}$$

$$B \approx \frac{1}{G_0} \frac{2x - j}{j4N} \tag{Appendix.90}$$

$$C \approx 2\pi fC_0x - 4NG_0 - j \left(\pi fC_0 + \frac{4NG_0}{2x - j} \right) \tag{Appendix.91}$$

$$D \approx 2\pi fC_0Z_0x - 4N - j\pi fC_0Z_0 \tag{Appendix.92}$$

7.4.2 Appendix 4.2: [ABCD] matrix representation of propagation path

Based on equivalent circuit star model of propagation path in section 3.3, [ABCD] matrix representation of propagation way can be obtained clearly:

$$A_{path} = D_{path} = \cos 2\theta \tag{Appendix.93}$$

$$B_{path} = C_{path} = j \sin 2\theta \tag{Appendix.94}$$

With
$$\theta = \frac{\pi fl}{v} \tag{Appendix.95}$$

Where l is the length of propagation path between two IDTs.

So, [ABCD] matrix representations of input IDT, propagation way and output IDT are obtained. They are cascaded as Figure Appendix.13:

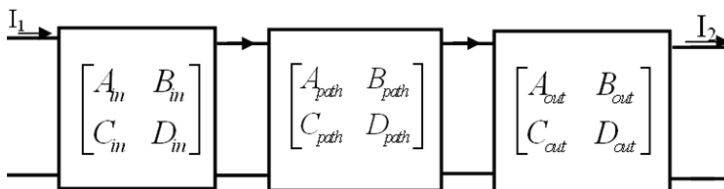


Fig. Appendix.13. Cascaded [ABCD] matrices of input IDT, propagation way and output IDT

And the [ABCD] equivalent matrix of SAW device is shown in Figure Appendix.14

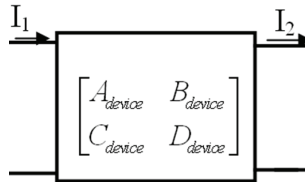


Fig. Appendix.14. [ABCD] matrix of SAW device

[ABCD] matrix of delay line SAW is

$$\begin{bmatrix} A_{device} & B_{device} \\ C_{device} & D_{device} \end{bmatrix} = \begin{bmatrix} A_{in} & B_{in} \\ C_{in} & D_{in} \end{bmatrix} \begin{bmatrix} A_{path} & B_{path} \\ C_{path} & D_{path} \end{bmatrix} \begin{bmatrix} A_{out} & B_{out} \\ C_{out} & D_{out} \end{bmatrix} \quad (\text{Appendix.96})$$

$$A_{device} = A_{in}A_{path}A_{out} + B_{in}C_{path}A_{out} + A_{in}B_{path}C_{out} + B_{in}D_{path}C_{out} \quad (\text{Appendix.97})$$

$$B_{device} = A_{in}A_{path}B_{out} + B_{in}C_{path}B_{out} + A_{in}B_{path}D_{out} + B_{in}D_{path}D_{out} \quad (\text{Appendix.98})$$

$$C_{device} = C_{in}A_{path}A_{out} + D_{in}C_{path}A_{out} + C_{in}B_{path}C_{out} + D_{in}D_{path}C_{out} \quad (\text{Appendix.99})$$

$$D_{device} = C_{in}A_{path}B_{out} + D_{in}C_{path}B_{out} + C_{in}B_{path}D_{out} + D_{in}D_{path}D_{out} \quad (\text{Appendix.100})$$

Where $[ABCD]_{in}$ is calculated from (Appendix.71), (Appendix.72), (Appendix.73) and (Appendix.74).

$[ABCD]_{out}$ is calculated from (Appendix.80), (Appendix.81), (Appendix.82) and (Appendix.83).

$[ABCD]_{path}$ is calculated from (Appendix.93) and (Appendix.94).

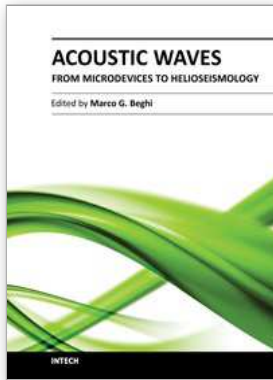
8. References

- [1] C.C.W.Ruppel, W.Ruile, G.Scholl, K.Ch.Wagner, and O.Manner, Review of models for low-loss filter design and applications, *IEEE Ultrasonics Symposium*, pp.313-324, 1994.
- [2] L.A.Coldren, and R.L.Rosenberg, Scattering matrix approach to SAW resonators, *IEEE Ultrasonics Symposium*, 1976, pp.266-271.
- [3] R.W.Newcomb, Linear Multiport Synthesis, McGraw Hill, 1966.
- [4] C.Elachi, Waves in Active and Passive Periodic Structures: A Review, *Proceedings of the IEEE*, vol.64, No.12, December 1976, pp.1666-1698
- [5] M.Hikita, A.Isobe, A.Sumioaka, N.Matsuura, and K.Okazaki, Rigorous Treatment of Leaky SAW's and New Equivalent Circuit Representation for Interdigital Transducers, *IEEE Transactions on Ultrasonics, Ferroelectrics, and Frequency Control*, Vol.43, No.3, May 1996.
- [6] L.F.Brown, and D.L.Carlson, Ultrasound Transducer Models for Piezoelectric Polymer Films, *IEEE Transactions on Ultrasonics, Ferroelectrics, and Frequency Control*, Vol.36, No.3, May 1989.
- [7] K.Hashimoto, and M.Yamaguchi, Precise simulation of surface transverse wave devices by discrete Green function theory, *IEEE Ultrasonics Symposium*, 1994, pp.253-258.

- [8] K.Hashimoto, G.Endoh, and M.Yamaguchi, Coupling-of-modes modelling for fast and precise simulation of leaky surface acoustic wave devices, *IEEE Ultrasonics Symposium*, 1995, pp.251-256.
- [9] K.Hashimoto, and M.Yamaguchi, General-purpose simulator for leaky surface acoustic wave devices based on Coupling-Of-Modes theory, *IEEE Ultrasonics Symposium*, 1996, pp.117-122.
- [10] K.Hashimoto, Surface Acoustic Wave Devices in Telecommunications, *Modelling and Simulation*, Springer, 2000, ISBN: 9783540672326.
- [11] P.M.Smith, and C.K.Campbell, A Theoretical and Experimental Study of Low-Loss SAW Filters with Interdigitated Interdigital Transducers, *IEEE Transactions on Ultrasonics, Ferroelectrics, and Frequency Control*, Vol.36, No.1, January 1989, pp.10-15.
- [12] C.K.Campbell, Modelling the Transverse-Mode Response of a Two-Port SAW Resonator, *IEEE Transactions on Ultrasonics, Ferroelectrics, and Frequency Control*, Vol.38, No.3, May 1991, pp.237-242.
- [13] C.K.Campbell, P.M.Smith, and P.J.Edmonson, Aspects of Modeling the Frequency Response of a Two-Port Waveguide-Coupled SAW Resonator-Filter, *IEEE Transactions on Ultrasonics, Ferroelectrics, and Frequency Control*, Vol.39, No.6, November 1992, pp.768-773.
- [14] C.K.Campbell, Longitudinal-Mode Leaky SAW Resonator Filters on 64° Y-X Lithium Niobate, *IEEE Transactions on Ultrasonics, Ferroelectrics, and Frequency Control*, Vol.42, No.5, September 1995, pp.883-888.
- [15] C.K.Campbell, and P.J.Edmonson, Conductance Measurements on a Leaky SAW Harmonic One-Port Resonator, *IEEE Transactions on Ultrasonics, Ferroelectrics, and Frequency Control*, Vol.47, No.1, January 2000, pp.111-116.
- [16] C.K.Campbell, and P.J.Edmonson, Modeling a Longitudinally Coupled Leaky-SAW Resonator Filter with Dual-Mode Enhanced Upper-Sideband Suppression, *IEEE Transactions on Ultrasonics, Ferroelectrics, and Frequency Control*, Vol.48, No.5, September 2001, pp.1298-1301.
- [17] J.Munshi, and S.Tuli, A Circuit Simulation Compatible Surface Acoustic Wave Interdigital Transducer Macro-Model, *IEEE Transactions on Ultrasonics, Ferroelectrics, and Frequency Control*, Vol.51, No.7, July 2004, pp.782-784.
- [18] M.P.Cunha, and E.L.Adler, A Network Model For Arbitrarily Oriented IDT Structures, *IEEE Transactions on Ultrasonics, Ferroelectrics, and Frequency Control*, Vol.40, No.6, November 1993, pp.622-629.
- [19] D.R.Mahapatra, A.Singhal, and S.Gopalakrishnan, Numerical Analysis of Lamb Wave Generation in Piezoelectric Composite IDT, *IEEE Transactions on Ultrasonics, Ferroelectrics, and Frequency Control*, Vol.52, No.10, October 2005, pp.1851-1860.
- [20] A APPENDIX. Bhattacharyya, Suneet Tuli, and S.Majumdar, SPICE Simulation of Surface Acoustic Wave Interdigital Transducers, *IEEE Transactions on Ultrasonics, Ferroelectrics, and Frequency Control*, Vol.42, No.4, July 1995, pp.784-786.
- [21] C.M.Panasik, and APPENDIX.J.Hunsinger, Scattering Matrix Analysis Of Surface Acoustic Wave Reflectors And Transducers, *IEEE Transactions On Sonics And Ultrasonics*, Vol.SU-28, No.2, March 1981, pp.79-91.
- [22] W.Soluch, Admittance Matrix Of A Surface Acoustic Wave Interdigital Transducer, *IEEE Transactions on Ultrasonics, Ferroelectrics, and Frequency Control*, Vol.40, No.6, November 1993, pp.828-831.
- [23] W.Soluch, Scattering Matrix Approach To One Port SAW Resonators, *IEEE Frequency Control Symposium*, 1999, pp.859-862.

- [24] W.Soluch, Design of SAW Synchronous Resonators on ST Cut Quartz, *IEEE Transactions on Ultrasonics, Ferroelectrics, and Frequency Control*, Vol.46, No.5, September 1999, pp.1324-1326.
- [25] W.Soluch, Scattering Matrix Approach To One-Port SAW Resonators, *IEEE Transactions on Ultrasonics, Ferroelectrics, and Frequency Control*, Vol.47, No.6, November 2000, pp.1615-1618.
- [26] W.Soluch, Scattering Matrix Approach To STW Resonators, *IEEE Transactions on Ultrasonics, Ferroelectrics, and Frequency Control*, Vol.49, No.3, March 2002, pp.327-330.
- [27] W.Soluch, Scattering Analysis Of Two-Port SAW Resonators, *IEEE Transactions on Ultrasonics, Ferroelectrics, and Frequency Control*, Vol.48, No.3, May 2001, pp.769-772.
- [28] W.Soluch, Scattering Matrix Approach To STW Multimode Resonators, *Electronics Letters*, 6th January 2005, Vol.41, No.1.
- [29] K.Nakamura, A Simple Equivalent Circuit For Interdigital Transducers Based On The Couple-Mode Approach, *IEEE Transactions on Ultrasonics, Ferroelectrics, and Frequency Control*, Vol.40, No.6, November 1993, pp.763-767.
- [30] K. Nakamura, and K.Hirota, Equivalent circuit for Unidirectional SAW-IDT's based on the Coupling-Of-modes theory, *IEEE Trans on Ultrasonics, Ferroelectrics, and Frequency Control*, Vol.43, No.3, May 1996, pp.467-472.
- [31] A.H.Fahmy, and E.L.Adler, Propagation of acoustic surface waves in multilayers: A matrix description. *Applied Physics Letter*, vol. 22, No.10, 1973, pp. 495-497.
- [32] E.L.Adler, Matrix methods applied to acoustic waves in multilayers, *IEEE Transactions on Ultrasonics, Ferroelectrics, and Frequency Control*, Vol.37, No.6, November 1990, pp.485-490.
- [33] E.L.Adler, SAW and Pseudo-SAW properties using matrix methods, *IEEE Transactions on Ultrasonics, Ferroelectrics, and Frequency Control*, Vol.41, No.5, September 1994, pp.699-705.
- [34] G.F.Iriarte, F.Engelmark, I.V.Katardjiev, V.Plessky, V.Yantchev, SAW COM-parameter extraction in AlN/diamond layered structures, *IEEE Transactions On Ultrasonics, Ferroelectrics, And Frequency Control*, Vol. 50, No. 11, November 2003.
- [35] M.Mayer, G.Kovacs, A.Bergmann, and K.Wagner, A Powerful Novel Method for the Simulation of Waveguiding in SAW Devices, *IEEE Ultrasonics Symposium*, 2003, pp.720-723.
- [36] W.P.Mason, Electromechanical Transducer and Wave Filters, second edition, D.Van Nostrand Company Inc, 1948.
- [37] W.P.Mason, Physical Acoustics, Vol 1A, Academic Press, New York 1964.
- [38] S.D.Senturia, Microsystem Design, Kluwer Academic Publishers, 2001, ISBN 0-7923-7246-8.
- [39] W.Marshall Leach, Controlled-Source Analogous Circuits and SPICE models for Piezoelectric transducers, *IEEE Transactions on Ultrasonics, Ferroelectrics, and Frequency Control*, Vol.41, No.1, January 1994.
- [40] D.A.Berlincourt, D.R.Curran and H.Jaffe, Chapter 3, Piezoelectric and Piezomagnetic Materials and Their Function in Transducers.
- [41] W.R.Smith, H.M.Gerard, J.H.Collins, T.M.Reeder, and H.J.Shaw, Analysis of Interdigital Surface Wave Transducers by Use of an Equivalent Circuit Model, *IEEE Transaction on MicroWave Theory and Techniques*, No.11, November 1969, pp.856-864.
- [42] C. K. Campbell, Surface acoustic wave devices, in *Mobile and Wireless Communications*, New York: Academic, 1998.

- [43] O.Tigli, and M.E.Zaghloul, A Novel Saw Device in CMOS: Design, Modeling, and Fabrication, *IEEE Sensors journal*, vol. 7, No. 2, February 2007, pp.219-227.
- [44] K.Nakamura, A Simple Equivalent Circuit For Interdigital Transducers Based On The Couple-Mode Approach, *IEEE Transactions on Ultrasonics, Ferroelectrics, and Frequency Control*, Vol.40, No.6, November 1993, pp.763-767.
- [45] M.Hofer, N.Finger, G.Kovacs, J.Schoberl, S.Zaglmayr, U.Langer, and R.Lerch, Finite-Element Simulation of Wave Propagation in Periodic Piezoelectric SAW Structures, *IEEE Transactions on Ultrasonics, Ferroelectrics, and Frequency Control*, Vol.53, No.6, June 2006, pp.1192-1201.
- [46] M. Hofer, N. Finger, G. Kovacs, J. Schoberl, U. Langer, and R. Lerch, Finite-element simulation of bulk and surface acoustic wave (SAW) interaction in SAW devices, *IEEE Ultrasonics Symposium*, 2002.
- [47] Online: <http://www.comsol.com/>
- [48] Online: <http://www.coventor.com/>
- [49] Online: <http://www.ansys.com/>
- [50] J.J. Campbell, W.R. Jones, A method for estimating optimal crystal cuts and propagation directions for excitation of piezoelectric surface waves, *IEEE Transaction on Sonics Ultrasonics*. SU-15 (4), 1968, pp.209-217.
- [51] E.Akcakaya, E.L.Adler, and G.W.Farnell, Apodization of Multilayer Bulk-Wave Transducers, *IEEE Transactions on Ultrasonics Ferroelectrics and Frequency Control*, Vol.36, No.6, November 1989, pp 628-637.
- [52] E.L.Adler, J.K.Slaboszewicz, G.W.FARNELL, and C.K.JEN, PC Software for SAW Propagation in Anisotropic Multilayers, *IEEE Transactions on Ultrasonics Ferroelectrics and Frequency Control*, Vol.37, No.2, May 1990, pp.215-223.
- [53] E.L.Adler, SAW and Pseudo-SAW Properties Using Matrix Methods, *IEEE Transactions on Ultrasonics Ferroelectrics and Frequency Control*, Vol.41, No.6, pp.876-882, September 1994.
- [54] K. A. Ingebrigtsen, Surface waves in piezoelectrics, *Journal of Applied Physics*, Vol.40, No.7, 1969, pp.2681-2686.
- [55] Y.Suzuki, H.Shimizu, M.Takeuchi, K.Nakamura, and A.Yamada, Some studies on SAW resonators and multiple-mode filters, *IEEE Ultrasonics Symposium Proceedings*, 1976, pp.297-302.
- [56] S.D.Senturia, *Microsystem Design*, Kluwer Academic Publishers, 2001, ISBN 0-7923-7246-8.
- [57] W.P.Mason, *Electromechanical Transducer and Wave Filters*, second edition, D.Van Nostrand Company Inc, 1948.
- [58] W.P.Mason, *Physical Acoustics*, Vol 1A, Academic Press, New York 1964.
- [59] W.R.Smith, H.M.Gerard, J.H.Collins, T.M.Reeder, and H.J.Shaw, Analysis of Interdigital Surface Wave Transducers by Use of an Equivalent Circuit Model, *IEEE Transaction on MicroWave Theory and Techniques*, No.11, November 1969, pp.856-864.
- [60] Y.Suzuki, H.Shimizu, M.Takeuchi, K.Nakamura, and A.Yamada, Some studies on SAW resonators and multiple-mode filters, *IEEE Ultrasonics Symposium Proceedings*, 1976, pp.297-302.
- [61] K.Nakamura, A Simple Equivalent Circuit For Interdigital Transducers Based On The Couple-Mode Approach, *IEEE Transactions on Ultrasonics, Ferroelectrics, and Frequency Control*, Vol.40, No.6, November 1993, pp.763-767.



Acoustic Waves - From Microdevices to Helioseismology

Edited by Prof. Marco G. Beghi

ISBN 978-953-307-572-3

Hard cover, 652 pages

Publisher InTech

Published online 14, November, 2011

Published in print edition November, 2011

The concept of acoustic wave is a pervasive one, which emerges in any type of medium, from solids to plasmas, at length and time scales ranging from sub-micrometric layers in microdevices to seismic waves in the Sun's interior. This book presents several aspects of the active research ongoing in this field. Theoretical efforts are leading to a deeper understanding of phenomena, also in complicated environments like the solar surface boundary. Acoustic waves are a flexible probe to investigate the properties of very different systems, from thin inorganic layers to ripening cheese to biological systems. Acoustic waves are also a tool to manipulate matter, from the delicate evaporation of biomolecules to be analysed, to the phase transitions induced by intense shock waves. And a whole class of widespread microdevices, including filters and sensors, is based on the behaviour of acoustic waves propagating in thin layers. The search for better performances is driving to new materials for these devices, and to more refined tools for their analysis.

How to reference

In order to correctly reference this scholarly work, feel free to copy and paste the following:

Trang Hoang (2011). SAW Parameters Analysis and Equivalent Circuit of SAW Device, *Acoustic Waves - From Microdevices to Helioseismology*, Prof. Marco G. Beghi (Ed.), ISBN: 978-953-307-572-3, InTech, Available from: <http://www.intechopen.com/books/acoustic-waves-from-microdevices-to-helioseismology/saw-parameters-analysis-and-equivalent-circuit-of-saw-device>

INTECH

open science | open minds

InTech Europe

University Campus STeP Ri
Slavka Krautzeka 83/A
51000 Rijeka, Croatia
Phone: +385 (51) 770 447
Fax: +385 (51) 686 166
www.intechopen.com

InTech China

Unit 405, Office Block, Hotel Equatorial Shanghai
No.65, Yan An Road (West), Shanghai, 200040, China
中国上海市延安西路65号上海国际贵都大饭店办公楼405单元
Phone: +86-21-62489820
Fax: +86-21-62489821

© 2011 The Author(s). Licensee IntechOpen. This is an open access article distributed under the terms of the [Creative Commons Attribution 3.0 License](#), which permits unrestricted use, distribution, and reproduction in any medium, provided the original work is properly cited.